OFFICE OF NAVAL RESEARCH TECHNICAL REPORT FOR

Grant No. N00014-95-WR-20027

PR NUMBER: 96PRO-3804 - Robert J. Nowak

Technical Report #14

MOLECULAR DYNAMICS STUDY OF INTERFACIAL ELECTRIC FIELDS

Prepared for Publication in
Electrochimica Acta
by
James N. Glosli
Lawrence Livermore National Laboratory,
University of California, Livermore, CA 94550
and
Michael R. Philpott
IBM Research Division, Almaden Research Center,
650 Harry Road, San Jose, CA 95120-6099

Abstract

Electric fields and potentials of an equilibrated assembly of ions and water molecules adjacent to a charged metal surface are calculated as a function of perpendicular distance z from the surface from data derived from molecular dynamics trajectories. The spatial distributions of atoms or molecules along direction z are found by ensemble averaging of trajectories followed by averaging with a localized function with a well defined length scale. Two methods were used calculate z dependent charge density distributions. In the first, to be called the atom method, the trajectories of charged atoms are averaged. In the second, called the molecule method, a Taylor expansion of charged atom positions relative to molecular centers is performed and the charge density separated into monopole, dipole, quadrupole, octopole,... components. These distributions are used to calculate the electric potential and in one example to study the progressive loss of structure due to water as the length parameter is scanned through the dimension of a water molecule. This latter result provides a link between simulations with detailed atomic modeling of intermolecular interactions and electric potentials derived from Gouy-Chapman theory. Illustrative examples are chosen from simulations of aqueous solutions of simple alkali halide electrolytes next to charged and uncharged flat metal surfaces. The smallest system has one ion and 157 water molecules, the largest 60 ions and 1576 water molecules.

MOLECULAR DYNAMICS STUDY OF INTERFACIAL ELECTRIC FIELDS

James N. Glosli

Lawrence Livermore National Laboratory,

University of California, Livermore, CA 94550

and

Michael R. Philpott

IBM Research Division, Almaden Research Center,

650 Harry Road, San Jose, CA 95120-6099

Abstract

Electric fields and potentials of an equilibrated assembly of ions and water molecules adjacent to a charged metal surface are calculated as a function of perpendicular distance z from the surface from data derived from molecular dynamics trajectories. The spatial distributions of atoms or molecules along direction z are found by ensemble averaging of trajectories followed by averaging with a localized function with a well defined length scale. Two methods were used calculate z dependent charge density distributions. In the first, to be called the atom method, the trajectories of charged atoms are averaged. In the second, called the molecule method, a Taylor expansion of charged atom positions relative to molecular centers is performed and the charge density separated into monopole, dipole, quadrupole, octopole,... components. These distributions are used to calculate the electric potential and in one example to study the progressive loss of structure due to water as the length parameter is scanned through the dimension

of a water molecule. This latter result provides a link between simulations with detailed atomic modeling of intermolecular interactions and electric potentials derived from Gouy-Chapman theory. Illustrative examples are chosen from simulations of aqueous solutions of simple alkali halide electrolytes next to charged and uncharged flat metal surfaces. The smallest system has one ion and 157 water molecules, the largest 60 ions and 1576 water molecules.

I. INTRODUCTION

In this paper we describe the calculation of electrostatic fields arising from ions and polar molecules in equilibrium distributions in front of charged metal electrodes. The focus is on fields within ten water molecule diameters of the electrode-aqueous electrolyte interface. Molecular dynamics simulations are used to calculate the trajectories of ions and polar molecules, which are time and space averaged in a manner to be described to get time independent distributions depending only on the coordinate z perpendicular to the surface. These averaged distributions are then used as the source terms in Maxwell's equations to calculate fields and potentials that are in a form that can be compared with potentials derived intuitively from electrochemical knowledge or the results of non simulation methods like that of Gouy-Chapman-Stern[1-4] theory or Henderson and coworkers more sophisticated correlation function technique[5]. These latter methods solve Poisson's equation with the Boltzmann ansatz and calculate from the charge distribution the electric field and potential across the double layer region. In our work examples are chosen from simulations of aqueous solutions of simple electrolytes next to charged metal surfaces that represent frequently encountered situations in adsorption from electric double layers. All sums of electrostatic interactions are evaluated without spatial cut-offs using the fast multipole method of Greengard and coworkers[6-9]

The cartoon in Figure 1 depicts the traditional view [10, 11] of the electric double layer in the thermodynamically stable region of electrode potential for a metal with a flat surface. The electric potential due to ions is schematically shown at top. We will show that near the surface this way of depicting the distance dependence of the potential is wrong because it neglects the contribution from oriented water molecules. In Figure 1 the labels IHP and OHP denote the inner and outer Helmholtz planes respectively. In the cartoon the compact part of the double layer contains an anion in physical contact with a flat surface and a cation two water molecules distant from the electrode as in the the model of Bockris, Devanathan and Müller[12]. The diffuse

part is symbolized by the labelled arrows which cover the region from the OHP to the bulk electrolyte region.

The calculation of the classical electric field of a set of charges is a well studied problem. Given a set of charges the electric field and potential can be found with arbitary high accuracy by a number of methods. In molecular dynamics and Monte Carlo simulations Ewald's method has been frequently used. However in systems large numbers (N > 200) of charged or polar species, Ewald methods are slow (time $t \propto N^{1.5}$) compared to the fast multipole method ($t \propto N$) and particle-mesh methods[13] ($t \propto N \log N$). The molecular dynamics simulations described in this paper would not be possible without the use of the fast multipole method to evaluate the long range electrostatic fields. Using the fast multipole method we have performed many simulations on systems containing 600 charged particles and a few simulations on larger systems containing 5000 charged particles and their electrostatic images.

Given that we are able to accurately evaluate long range electrostatic interactions in a molecular dynamics simulation, the next step is the calculation of local electric fields from time averaged charge distributions. This is the main task of the present paper. We concentrate on two methods to calculate time and space averages of charge source functions, and the corresponding electric fields and potentials. The first method, to be called the atom charge method, uses the positions of the atoms and the charge or partial charge of the atoms to calculate a time independent electric charge density. After making averages parallel to the surface this technique yields results equivalent to that described by Wilson, Pohorille and Pratt[14, 15], based on the derivation given in Landau and Lifshitz[16]. The second method (called the molecule method) considers the system in a fundamentally different way. It views the world as a collection of charged or polar molecules. It uses a Taylor series expansion of charged atom coordinates relative to an origin on the molecule to express the electric source in terms of a sequence of electric multipole (monopole, dipole, quadrupole, octopole,...) polarization source densities. This method follows the de-

scription given in standard texts such as Jackson[17], which is based in part on the lucid description in the paper by Russakoff[18]. By this second method the contribution to the electric field and potential of monopole, dipole, quadrupole, octopole,... moments of the molecules can be calculated separately in a systematic way, and could in principle be used to input experimentally measured values of electric multipole moments. Each of the two methods provides its own particular insight in the computation of the fields.

To illustrate the calculation of the fields and potentials we choose examples from on going work in simulations of aqueous electrochemical interfaces that typify general classes of behaviour. All the systems were composed of water and monovalent ions adjacent to a metal surface. The examples chosen from small scale simulations are: a non contact adsorbed Li^+ ion, a contact adsorbed I^- ion, a neutral solution of Li^+ and I^- (anion contact adsorbed), a neutral solution of Li^+ and F^-, and Li^+ and two iodides $2I^-$ (cation attracted to contact adsorbed anions). As an example of a larger calculation that shows that some of the main features in the small simulations are also found in calculations ten times larger is given at the end of the paper. In this example we discuss a 1M NaCl salt solution in front of a charged electrode. In this simulation the region of electrolyte that screens the charge on the electrode and the bulk solution are evident.

In our smallest simulations the cell size (L = 1.862 nm) is too small for us to be confident that we can do more than describe the average electric field between the metal and the OHP. The decay of the average electric field to zero at the non metal boundary is the result of charge neutrality in the immersed electrode model. Consequently in the smaller simulations we focus primarily on the interfacial fields within the first three or four water molecules, corresponding to a distance up to about one nm from the electrode. In the large simulation with a cell (L = 3.74 nm) containing 5000 charges[19], the distribution of ions from the zone where the screening of the charged metal occurs, all the way to the 'bulk' electrolyte is observed. In this case we can more confidently interpret the decay of field and potential found in the calculations and

identify what corresponds to the diffuse region of the electric double layer. Traditionally the structure of the compact region where ions contact adsorb is thought of as being static and resembling a capacitor of atomic separations. Our model permits the ions to move in and out freely from the diffuse layer and to contact adsorb and desorb. We note that Henderson and coworkers[20] in their work solving the Ornstein-Zernike equation for the electrode-electrolyte interface have shown (as does the work presented here) that there is no sharp division between the diffuse and inner layers, in contrast to the ideas conveyed by the pictures in many textbooks.

We summary the goals of the present work are as follows. First, the calculation of averaged electric field and potential for systems of electrochemical interest. Second, to contrast the atom and molecule methods of calculating charge densities and potentials. Third, to qualitatively analyse deviations in the electric potential from the curve for ions in a dielectric fluid interms of distribution of solvent and ions near the metal surface.

We close this section with a brief mention of important parts of the physics that are still missing. First there is no feature that permits explicit consideration of the metal surface topography and conduction electron densities at the surface. For example, one can go much further and use jellium models or jellium with embedded ions but this is beyound the scope of the current study. Halley and coworkers[21-23] have developed theories based on jellium electrode models of the charged metal surface and adjacent solution that accounts for aspects of measured capacitance vs. potential curves. Cluster calculations have been used to obtain metal-water and metal-ion potentials for use in molecular dynamics simulations that introduce aspects of metal surface corrugation[24-26], [27-29], [30-34], [35-37]. Second the are no effects due to electronic polarizability or geometric distortions of molecules in the high electric fields of the double layer.

II. MODELS AND METHODS.

A. The Immersed Electrode Model.

When the electrode potential is altered and charge flows onto the electrode, the composition of the electrolyte next to the electrode adjusts to screen the new charge on the electrode. For dilute solutions (< 0.1 M) a rough estimate of the screening layer thickness is $d = \kappa^{-1}$, where κ is the Debye-Huckel screening constant. According to the Gouy-Chapman theory[10] the concentration of monovalent ions has fallen to e^{-1} of its 'surface' value at a distance d from the electrode given by

$$d = \sqrt{\left(\frac{\varepsilon kT}{8\pi e^2 n_b} \right)} \qquad [2.1]$$

Here ε is the macroscopic dielectric constant of the solvent, and n_b is the concentration of the ions in the bulk. Typical values of d are: 3.1 nm for 0.01 M, and 0.96 nm for 0.1 M. At higher salt concentrations outside the range of the derivation of this formula we get 0.55 nm for 0.3 M, and 0.31 nm for 1 M salt solutions. The formula provides some rough measure perhaps even within a factor 2 (the effective dielectric constant of water near the electrode may be ten times smaller than in bulk[38]) of the double layer thickness even though the basis of the derivation is not valid. These brief considerations suggest we can use molecular dynamics to simulate an immersed electrode when the salt concentration is about 0.3 M or larger by including the adjacent electrolyte region out to a thickness of about ten water molecules. In this paper we do this first for a small cell about five water molecules thick, expecting only to be able to model the so-called inner part of the double layer where contact adsorption occurs. Later we study a cell about 10 waters thick and are able to identify a region in space that has bulk-like properties, lending support to the immersed electrode model as we use it. Our immersed electrode model

consists of a layer of electrolyte between two walls. The wall on the left carries no charge it is simply a restraining wall and ideally would allow a continuous transition to the bulk electrolyte region. The complete system of electrolyte and electrode (always on the right hand side in all the Figures of this paper) is neutral. The approach is useful because it reduces the number of water molecules in the calculation, and because there is only one metal surface, there is only one electrostatic image plane. Finally we point out that in our system the electrical properties of the system are due to three layers. The vacuum half space occupying: $-\infty < z < -½L$; the xy periodically replicated simulation cells: $-½L < z < ½L$; and the metal half space: $½L < z < \infty$. More details and discussion of the immersed electrode model are found elsewhere[39].

B. Models for water and ions.

In the smaller scale simulations reported here we used the parameters of the Stillinger[40, 41] ST2 water model and the interaction parameters with alkali metal ions and halide ions developed by Heinzinger and coworkers[24]. The ST2 water molecule model consists of a central oxygen atom surrounded by two hydrogen atoms and two massless point charges (PC) in a rigid tetrahedral-like arrangement. The charges on the particles are q_H=0.23570lel, q_{PC}=-q_H, and q_O =0. The alkali metal and halide ions are non-polarizable Lennard-Jones atoms with point mass and charge. The atom-atom interaction parameters are taken from Heinzinger's review[24]. In the larger simulations with a 3.74 nm wide cell containing 1M NaCl solution the SPCE water model was used primarily because this water model has fewer charges (three compared to four for ST2) and requires less time to compute the electrostatics. The Lennard-Jones potential between the atoms of each molecule was smoothly cut-off at distances of $R = 0.68$ nm.

C. Molecule-Wall and Ion-Wall Potentials.

There are two walls. The simplest is the uncharged restraining non metallic wall on the left hand side in Figures 2 - 15. It restrains the fluid by a 9-3 potential. The metal wall, on the right hand side, is represented by two superimposed potentials. The first is a 9 - 3 potential to represent

both the Pauli repulsion and dispersive attractive interactions. The second potential is an electrostatic image potential that describes the interaction between a charge in the electrolyte and the conduction electrons of the metal. In the calculations described here the image plane and origin plane of the 9-3 potential were coincident. This is equivalent to choosing the image plane and the nuclear plane of the metal surface to be the same. This is acceptable in our scheme because the Lennard-Jones core parameters σ are all large and the 'thickness' of the repulsive wall is also large (ca. 0.247 nm). The atom-surface interaction parameters describing interaction with nonconduction electrons were chosen to be the same as those of Lee at al[42], $A=17.447\times10^{-6}$ kJ(nm)^6/mole and $B=76.144\times10^{-3}$ kJ(nm)^3/mole for O, I ion and Li ion. The A and B parameters for H and PC were set to zero for water molecules. Note that in this model the adsorption well depths of the Lennard-Jones wall potentials is a few kcal/mole, similar to kT at room temperature, and therefore pretty whimpy.

D. Advantages of the Fast Multipole Method.

Simulations of aqueous electrolyte solutions using molecular dynamics and Monte Carlo methods require the evaluation of the superimposed Coulomb fields of thousands particles (a 5 nm cube of water contains about 12,500 atoms). In this paper we use the fast multipole method (fmm) of Greengard and Rokhlin[6-9] to evaluate the electric fields acting on the charged particles during the computer simulation. A number of methods are in use to calculate or approximate long range Coulomb fields. Friedmann and Honig[43] have surveyed some of empirical dielectric recipes in use in biological simulations. For example recipes like the Hingerty function [44] and other distance dependent dielectric 'constants' [45, 46] have been used in simulations of proteins. Direct summation with a cut off after about 1.00 nm is common in many commercially available codes like Charmm[47] and Amber[45, 48]. There are a number of plane wise summation methods from crystal physics[49]. For homogeneous systems the reaction field method of Barker [50] is simple and easy to use. This method is not easily applied to liquid-solid interfaces though at-

tempts to extend it have been described [51, 52]. The Ewald method [53-55] has been extensively used when rigor and accuracy are needed. Ewald's summation crudely applied is proportional to N^2 and at best $N^{3/2}$ where N is the number of charges. The fast multipole method (fmm) developed by Greengard and Rokhlin [6-9] is an order N algorithm, and consequently is the only viable method for very large simulations. The fmm technique is attractive because of the ease of implementation of a variety of boundary conditions such as periodic, Dirichlet, Neumann and mixed boundaries and because an adaptive version of the algorithm is available [8] in which regions of low or no charge density are not subdivided when the charge count falls below a specified integer.

III. ELECTROSTATICS OF ELECTROCHEMICAL CELLS

There are many ways that electric fields and potentials can be calculated. For example, at every time step we use the fast multipole method to compute the electric forces acting on every charged particle in the system. We could take the electric field evaluated at a specified particle, say an O atom, at a given instant of time and then either allow the molecule to move and average the field at regular intervals or confine the atom to a spatial well that would then be transported so as to sample all space. This would clearly be useful for interpreting experiments like NMR, but is not in the spirit of Gouy-Chapman theory which attempts to solve the Poisson equation using a Maxwell-Boltzmann ansatz for local charge fluctuations. It is not pursued further here. Instead in this section we describe two methods for getting source distributions to be used to calculate averaged electric fields and potentials for comparison with other theoretical methods which are in the spirit of Gouy-Chapman approach. The first method assumes that the atoms are fundamental objects and uses the charge or partial charge on each atom and the three space coordinates of each atom recorded at regular time separations (usually 0.5 or 1 ps) as input into the generation of a charged source distribution. We call this the atom approach. The only source term is the charge density function in vacuum. Without any local spatial averaging this point of view is similar to that followed by Wilson, Pohorille, and Pratt[14, 15]. The second way, to be called the molecule method, assumes that the system is a collection of molecules that have internal electrical structure. These are inherently more complex objects than atoms. To specify the electrical properties we need space coordinates, orientations and electrostatic multipole moments for each molecule in the system. The approach we follow can be found in the clearly written article by Russakoff[18], or the treatise by de Groot and Suttorp[56], both sets of authors derive a set of macroscopic equations from Maxwell's equations in vacuum for point charged particles. Their approach is summarized in a number of standard texts[17]. We note that though the dynamics are uniquely defined by the models we use, the time independent average fields

and potentials that are calculated are not unique because we can broaden the point charge distributions inside the ions and molecules in a spherically symetric way and so long as the broaden distributions stay well inside the Lennard-Jones spheres (so that distributions on different molecules do not overlap) the the dynamics are unchanged. This means we can smooth some of the averages within limits set by geometry of the models and the energetics of collisions. This point was clearly recognized by Wilson, Pohorille and Pratt[14, 57] in their interesting discussion of the properties of the vacuum-water surface.

The atom method uses the distribution of point charges in vacuum. Consider the set of point charges without regard for whether they originate from neutral water molecules or charged ions. In this case the source term for Maxwell fields in vacuum is the microscopic charge density

$$\rho_I(\mathbf{r},t) = \rho_{metal}(\mathbf{r},t) + \rho_{atoms}(\mathbf{r},t). \qquad [3.1]$$

Here

$$\rho_{metal}(\mathbf{r},t) = \rho_{metal}(x,y,t)\delta(z - \tfrac{1}{2}L), \qquad [3.2]$$

and

$$\rho_{atoms}(\mathbf{r},t) = \sum_{j=1}^{N_{atoms}} q_j \delta(\mathbf{r} - \mathbf{r}_j(t)'), \qquad [3.3]$$

where N_{atoms} is the number of atoms in the simulation cell and $\mathbf{r}_j$ is the position of the j-th atom. The surface charge density on the metal $\rho_{metal}(x,y,t)$ is time dependent because it depends on the position of the atomic charges. All the charge in the system is described by ρ_I.

We can subject this charge density to local space averaging using a test function. Let $f(\mathbf{r})$ be a real positive function localized around $\mathbf{r} = 0$. We define the local spatial average of $F(\mathbf{r}, t)$ by

$$<F(\mathbf{r}, t)> = \int d\mathbf{r}' f(\mathbf{r}')F(\mathbf{r} - \mathbf{r}', t). \qquad [3.4]$$

The time average

$$\overline{F}(\mathbf{r}) = \lim_{t \to \infty} \frac{1}{t} \int_0^t < F(\mathbf{r}, t')> dt' \qquad [3.5]$$

can be replaced by an average over configurations at different times

$$\overline{F}(\mathbf{r}) \approx \frac{1}{N_{configs}} \sum_{i=1}^{N_{configs}} <F(\mathbf{r}, t_i)>. \qquad [3.6]$$

The systems we consider have translational invariance in the xy plane. The function $\overline{F}(\mathbf{r})$ is a function of z only. In light of this we consider only test functions which are functions of z. We use two test functions, a bin-like test function

$$f(\mathbf{r}) = \begin{cases} 1/g & , \quad |z| < \frac{1}{2}g \\ 0 & , \quad |z| > \frac{1}{2}g \end{cases} \qquad [3.7]$$

and a localized one dimensional Gaussian function

$$f(z) = (\pi g^2)^{-1/2}\, e^{-(z/g)^2}. \qquad [3.8]$$

The metal surface charge density $\rho_{metal}(x,y,t)$ is replaced by the averaged image charge density which is a constant. The metal image charge is denoted by $\overline{\rho}_{metal}$. After we have averaged over the many spatial configurations from the molecular dynamics calculation we obtain a z dependent charge density profile given by

$$\overline{\rho}_I(z) = \overline{\rho}_{metal}\delta(z - \tfrac{1}{2}L) + \overline{\rho}_{atoms}(z) \qquad [3.9]$$

where as in Eq.(3.6)

$$\overline{\rho}_{atoms}(z) = \frac{1}{N_{configs}} \sum_{i=1}^{N_{configs}} <\rho_{atoms}(\mathbf{r}, t_i)>. \qquad [3.10]$$

After substituting explicitly for the test function we get

$$\overline{\rho}_{atoms}(z) = \frac{1}{N_{configs}} \sum_{i=1}^{N_{configs}} \sum_{j=1}^{N_{atoms}} q_j f(z - z_j(t_i)) \qquad [3.11]$$

The electric field is given directly by integrating the vacuum Maxwell's equation. Since we have already averaged over the xy plane the electric field normal to the surface is given by

$$\overline{E}_{I,z}(z) = \frac{1}{\varepsilon_0}\int_{-\infty}^{z} dz'\,\overline{\rho}_I(z') \qquad [3.12]$$

The electric potential is given by a second integration

$$\overline{\Phi}_I(z) = -\frac{1}{\varepsilon_0}\int_{-\infty}^{z} dz'\overline{E}_{I,z}(z') \qquad [3.13]$$

The second approach views the system as a collection of molecules (labels n, positions $\mathbf{r}_n$) composed of atoms (label b, position $\mathbf{r}_{nb}$, charge q_{nb}). The charge density of the system is:

$$\rho_{II}(\mathbf{r},t) = \rho_{metal}(x,y,t)\delta(z - \tfrac{1}{2}L) + \rho_{mol}(\mathbf{r},t) \qquad [3.14]$$

where ρ_{metal} is the same charge density on the metal surface as in the atomic method, and

$$\rho_{mol}(\mathbf{r},t) = \sum_{n=1}^{N_{mol}} \rho_n(\mathbf{r},t). \qquad [3.15]$$

Here N_{mol} is the total number of molecules in the system,

$$\rho_n(\mathbf{r},t) = \sum_{b=1}^{N_{na}} q_{nb}\delta(\mathbf{r} - \mathbf{r}_n - \mathbf{r}_{nb}), \qquad [3.16]$$

is the charge density of the n th molecule. The number of atoms in the n th molecule is N_{na}, and $\mathbf{r}_{nb}$ is the position of the charge q_{nb} measured from the center $\mathbf{r}_n$ of the n th molecule.

Next we perform explicit local spatial averaging with a test function and take the ensemble average. These steps are formally the same as described for the atom method. For each molecule label n we take the average with respect to the test function $f(z)$, then make a Taylor expansion of atomic coordinates $\mathbf{r}_{nb}$ relative to the molecular centers $\mathbf{r}_m$. This yields the following expression for the averaged charge density by the molecule method

$$\overline{\rho}_{mol}(z) = \overline{\rho}(z) - \frac{d}{dz}\overline{P}_z(z) + \frac{d^2}{dz^2}\overline{Q}_{zz}(z) - \frac{d^3}{dz^3}\overline{O}_{zzz}(z) + \cdots \qquad [3.17]$$

where

$$\overline{\rho}(z) = \frac{1}{N_{configs}} \sum_{i=1}^{N_{configs}} \sum_{m=1}^{N_{mol}} f(z - z_m(t_i)) \sum_{b=1}^{N_{ma}} q_{mb} \qquad [3.18]$$

$$\overline{P}_z(z) = \frac{1}{N_{configs}} \sum_{i=1}^{N_{configs}} \sum_{m=1}^{N_{mol}} f(z - z_m(t_i)) \sum_{b=1}^{N_{ma}} q_{mb} z_{mb}(t_i) \qquad [3.19]$$

$$\overline{Q}_{zz}(z) = \frac{1}{N_{configs}} \sum_{i=1}^{N_{configs}} \tfrac{1}{2} \sum_{m=1}^{N_{mol}} f(z - z_m(t_i)) \sum_{b=1}^{N_{mb}} q_{mb} z_{mb}(t_i) z_{mb}(t_i) \qquad [3.20]$$

$$\overline{O}_{zzz}(z) = \frac{1}{N_{configs}} \sum_{i=1}^{N_{configs}} \frac{1}{6} \sum_{m=1}^{N_{mol}} f(z - z_m(t_i)) \sum_{b=1}^{N_{mb}} q_{mb} z_{mb}(t_i) z_{mb}(t_i) z_{mb}(t_i) \qquad [3.21]$$

Here the charge density in the second method has been resolved into contributions from monopoles (ions only in this paper), dipoles, quadrupoles, octopoles, and higher order terms. In principle, experimental moments can be substituted for dipoles, quadrupoles,.. where these are known.

In the following sections we report simulations designed to typify general electrochemical systems. The distributions displayed in most of the Figures were calculated using a one dimensional binning function with width 0.004655 nm. In one case to be described in next section we discuss the effect of changing the size of the region averaged from smaller (.03 nm) to larger than the dimension of a water molecule.

IV. ALKALI METAL ION

This section describes molecular dynamics calculations with one Li^+ cation and 157 ST2 water molecules against a metal surface. The simulation cell is periodically replicated in the xy plane parallel to the metal surface. The simulation was run for 2500 ps, the first 100 ps of which were used to equilibrate the system. The charge on the electrode is the image charge -lel. At any instant this charge is not uniformily distributed across the electrode but localized on the surface in such a way as to produce the same electric field and potential as the electrostatic image of the lithium ion and all the water molecules. The field acting on the lithium ion comes from all the water molecules in the cell, all water and ions in xy periodically replicated cells, and all of the electrostatic images of the contents of all cells in the image plane of the metal. We emphasise again that in this calculation as in all the others descibed in this paper no electrostatic interaction is truncated. Figures 2 and 3 show the probability density profiles averaged over the xy direction and electrical potential calculated by the two ways described in section III. Note that in Figure 2 the probability of finding the ion and water have scales differing by fifty. Also plotted in Figure 2 is the total charge density by the atomic method. The bin size is L/400 = 0.004655 nm where L is the edge length of the simulation cell.

In Figure 2 we see that the Li^+ ion mass center mapped out a diffuse-like region between -0.6 and 0.4 nm. The lithium Li^+ ion has the smallest ionic radius of all the monovalent cations. Consequently it's hydration shell is very strongly bound making it more difficult for this ion to contact adsorb on the electrode. The asymmetry of the distribution may well be affected by the small width of the cell and consequently no significance is attached to its shape other than it is diffuse in nature. There may possibly be an hydrophobic plating of the ion to the left hand interface. On the metal side the ion rarely approached closer than 0.3 nm to the repulsive part of the wall potential shown by dashed line at 0.68 nm in Figure 2. This is approximately the average of the separate σ parameters for Li^+ and O_ST2 suggesting that lithium ion remains fully

hydrated at the metal surface, and that though surface water restricts the approach of the ion to the metal it does not exclude it. This behaviour of lithium ion is more like that postulated in the Grahame's picture of the double layer[58], than say the Bockris model[12]. To confirm such behaviour would require extending the simulation over many nanoseconds, or performing umbrella sampling[59]. This particular aspect of the problem is not pursued further here.

The water profile shows some new structure not seen in water without ions[39, 60]. Most interesting is the leading peak (closest to the metal surface) at ca. 0.68 nm due to a few localized water molecules. The orientation of these localized water molecules can be ascertained from the H_ST2 and PC_ST2 probability distributions (not shown here). The protons on these molecules give rise the distinct peak at ca. 0.75 nm in the H_ST2 distribution. In the PC_ST2 distribution (not shown) there is peak at ca. 0.625 nm that is enhanced more than the second peak in the H_ST2 profile which is at ca. 0.6 nm. The first water peak at ca. 0.68 nm lies between the first H and PC peaks measured from the metal surface. It appears therefore that some of the localized water molecules have one proton pointing at the electrode.

The atomic charge density profile in Figure 2 is dominated by neutral water. The large oscillation centered near 0.70 nm is due to partially oriented water. The main positive peak at ca. 0.75 nm is due to protons attracted to the metal by their images and the image field of the lithium ion. There are smaller oscillations in charge profile further from the surface that are more clearly seen if the distribution is smoothed. These tend to follow the oscillations in the water density probability in Figure 2. The actual lithium charge density is buried under the contribution from the water when the bin size is 0.004655 nm.

Figure 3 shows the electric potential across the cell calculated by the atomic charge method, and by the molecular method with systematic inclusion of higher electrostatic multipoles. For clarity the dashed vertical line denoting the point z = 0.628 nm where the wall potential goes through zero has been omitted except for the tick mark on the x axis. Since all the curves go off scale

near z = 0.682 nm all the data for z > 0.4 nm have been plotted again on a larger scale and are shown in the right hand panel. Note too that in this right hand panel the monopole curve m (broken curve) is scaled by 0.1 to distinguish it from the other curves. The notation in the figures is m = monopole, d = dipole, q = quadrupole. When m and d contributions are combined the curve is labelled m+d. When m, d and q contributions are combined the curve is labelled m+d+q. Only when three multipoles are included (m+d+q curve) do the potentials calculated by the two methods agree reasonably. Due to the small size of the bin it is necessary to include more higher multipoles before the atom and molecular methods agree quantitatively. The monopole contribution m (dashed line in Figure 3) due to lithium ion alone drops monotonically as expected for the potential inside a capacitor where the charge on the left is in a diffuse layer spatially separate from the charge on the right plate (metal) at z = 0.931 nm. Adding the dipole completely changes the potential (see m+d curve). The water molecules very effectively screen the field inside the capacitor, except for the region z > 0.68 nm where the water distribution drops rapidly to zero. Adding the quadrupole (also from water only) term brings the atomic and molecular calculations into some measure of agreement (note that the atomic and m+d+q potentials are off set by 0.04 in Figure 3). The quadrupole contribution to the potential is a negative constant in the region away from the wall potential. This occurs because its contribution to the charge $<\rho_{mol}(\mathbf{r},t)>$ contains a double derivative in space coordinates. The differences are greatest at the surfaces where the atomic method traces charge density smoothly whereas the molecular method, based on an expansion about molecular centers, requires many high multipoles to describe the field.

The variation in potential is rapid near the metal and Figure 3 shows this variation for the atomic and m+d+q approximation scaled by a factor 0.1. After adjusting for the offset of 0.04 the two curves become identical for z > 0.8 nm as expected for a region containing no molecules or ions. Between 0.6 and 0.75nm the difference between the methods are largest due the difference in

source terms. The dangers of omitting higher multipole was clearly pointed out by Wilson, Pororille and Pratt[14, 57] for water without ions.

Finally we return to the asymmetry in the lithium ion distribution. There are effects due to system size and ion-ion correlation. We have repeated some of the calculations with two lithium ions and 598 water_ST2 molecules for a few hundreds of picoseconds. The water structures appear almost exactly as in the smaller simulations. The lithium probability $\rho(z)$ for the two ion system is spread across most of the cell in a diffuse zone with a moderate bias towards the metal side of the cell. This result is satisfying in that no peculiar or pathological features are revealed implying that the smaller calculations can give usefully insight into water structure within about two water layers (ca. 0.6 nm from the point where the wall potential becomes repulsive at z=0.68 nm.).

We close this section with a discussion of changing the length scale over which the test function averaging is performed. The lithium system is chosen because the ion occupies a diffuse region and does not contact adsorb on the electrode. The initial smearing of ion charge by the localized gaussian average does not overlap the metal surface region so that changes near the metal reflect averaging the local distributions. Figure 4 shows the result of changing the size of the length scale when gaussian averaging is performed. It shows that as the averaging length scale increases the atom potential loses features at the scale of a water molecule. The parameter g (in nm units) is the width of the function $f_g(z)$ defined in Eqn.(3.8). There are two families of curves, the broken lines are for the atom (method I) potential with g = .03, .1, .3 and 1.0. Though hardly apparant because of the factor x20 in ordinate scale, the atom potential with g = .03 is close in numerical value to the atomic potential shown previously by the dotted curve in Figure 3. The g = 1.0 is extreme because it is close to half the box edge ½L = .931 nm. The behaviour of the g = 1.0 monopole shows there is some smeared charge beyond the left hand wall. What Figure 4 demonstrates is that as the size of the region averaged is increased from g = .03 nm (.1 x water

molecule dimension) to g = 1.0 nm (3 x water molecule dimension) the structure in the electric potential near the surface due to the water profile is lost. The total potential becomes monotonic and resembles the family of monopole potential curves calculated using the monopole charge distribution. Since the component of the water dipole perpendicular to the surface is not averaged to zero the atom potential at the surface remains smaller in magnitude. The macroscopic dielectric polarization remains and reduces the value of the surface potential by roughly an order of magnitude (curves for g = .3 nm). As expected the monopole potentials are not as sensitive to the value of the width g as the atomic potentials. This is an important qualitative result because it shows the transition from the microscopic scale, where surface water oscillatory structure dominates the potential, to macroscopic scale behaviour where water contributes a simple scaling of the electric potential.

V. IODIDE ION

In this section we describe simulations for one iodide anion I^- and 157 water molecules interacting with a metal surface. In practise it was found not necessary to run the simulation beyond 500 ps because the ion adsorbed on the metal after approximately 10 ps and remained there. However for consistency with the other simulations reported in this paper the calculation was allowed to run for 1000 ps. As in the case of lithium the first 100 ps were used to allow the system to equilibrate and were excluded from any statistical analyses. When the ions and water are described by the Heinzinger parameter set[24] we have shown in previous publications that: i) in fields of one GV/m all the halide ions except fluoride contact adsorbed on non-metal (surface with no electrostatic image interactions) electrodes[61], and ii) that similar behaviour occurred for the model of the metal used here when there was an unscreened external field of 1 GV/m pulling the ion to the surface[62].

Figures 5 and 6 show the probability density distributions and electric potential for the iodide system. Figure 5 shows the iodide ion distribution peaked at ca. 0.7 nm closer to the electrode than where the wall potential becomes positive at 0.68 nm. Compared to the previous example (lithium ion Figure 2) there is less structure in the water and in the H_ST2 and PC_ST2 component distributions (not shown). In fact apart from a small peak at 0.65 nm the distribution resembles water without ions in zero applied field[39, 62]. The atomic charge distribution displays a medium positive peak at ca. 0.65 nm (H_ST2) and two negative peaks at ca. 0.7 nm (iodide), and ca. 0.75 nm (PC_ST2).

The Figure 6 shows the electric potential calculated by the two methods. All components go off scale near z = 0.682 nm, and are plotted for z > 0.65 nm on a reduced scale (x0.2 in the right hand panel). The monopole potential m (broken curve) due to the iodide alone, is zero except close to the wall where the iodide is localized. There it changes swiftly from 0 to a high positive value corresponding to an electric field E_{ion} of approximately -5 GV/m. The absense of an

electric field due to iodide ions means there is little or no reaction from the water molecules and they are less ordered between -0.6 nm and 0.4 nm, and what ordering there is comes from the presence of the surfaces. In Figure 6 the m+d curve for combined monopole and dipole potentials shows a weaker variation compared to lithium ion. This means that before z = 0.4 nm the charge on the electrode is completely shielded. The curves of the atomic and m+d+q potentials overlap well for z < 0.4 nm due primarily to the water quadrupole contribution.

VI. NEUTRAL SOLUTIONS. POTENTIAL OF ZERO CHARGE

In this section we compute the properties of a neutral solution of LiI comprised of one Li ion and one I ion and 156 water molecules in the simulation cell, and compare it to the case of LiF with the same number of water molecules. There is no net attractive electric field on either ion because the total electrostatic image charge on the metal is zero. The two systems are quite different because iodide contact adsorbs on the metal and creates a surface localized electric dipole and field. Because the aqueous phase is neutral this simulation models a system at the potential of zero charge. This potential does not have to be zero, it will be very small if the charge distribution in the aqueous subphase is everywhere almost zero. The potential of zero charge is considered the natural reference point from which to measure electrode potentials. The measurement of change of surface tension of liquid metals with electrode potential is the only reliable direct method[63] of determining the PZC. The calculation of electric field and potential using the atom charge distribution have been published[64] so in this section we focus on comparing the atom calculations with the molecular method to gain further insight. Figure 7 displays the most important density profiles for the LiI system, and Figure 8 shows the various components of the electric potential.

In Figure 8 we note that the monopole potential m drops steeply as it passes through the diffuse layer of lithium ion (much as it did in the case of one lithium ion) because the iodide adsorbed on the metal acts like the second plate in a capacitor. The m+d curve shows that the water dipoles orient in the ion field and shield the ions from each other accept close to the metal. As in the previous two examples the water quadrupole shifts the electric potential to lower values by a constant amount. Note that the shift in potential from vacuum to metal, which measures the potential of zero charge, depends on the net dipole moment of the system[65]. The atomic and molecular methods give similar results. Closer results requires the inclusion of octopole and higher moments which contribute most near the surface.

We have also performed simulations on LiF under the same conditions that mimic the potential of zero charge. Figure 9 shows the probability distributions. In neutral LiF solution in contrast to LiI solution neither ion adsorbs on the electrode and both are comingled into a diffuse layer that is predominantly neutral across the system. The water distribution looks like water between uncharged plates. Figure 10 displays the electric potentials. As expected the contact potential was calculated to close to zero since the net dipole moment is very small. The monopole potential m shows a minimum related to the apparant bimodal distribution of the lithium ion. The water dipole orients to reduce the local electric field to a small value, with the result the curve m+d shows weak changes across the film. Adding the quadrupole in m+d+q shifts the whole potential downwards bringing it into close correspondence with the result of the atomic method of calculation. For $z < 0.4$ nm the atomic and m+d+q potentials are similar in shape and value. Higher multipole contribution to the molecular method are needed to bring it into closer correspondence to the atom method near the metal surface.

VII. LITHIUM CATION 'COADSORBED' WITH IODIDE IONS.

In this simulation we explore another important aspect of the adsorption of ions on metal electrodes, namely the ability of strong contact adsorbers like iodide ions I^- to adsorb on positively charged electrodes in sufficent excess to change the sign of the charge at the interface as observed by an ion located in the diffuse layer. In the case under consideration cations will be attracted out of the diffuse layer to compensate the excess negative charge at the interface. The interface can develope a layered structure of alternating charges. First there is positively charged metal, then a narrow layer of contact adsorbed negative ions, and then a layer of compensating cations. In real systems this compensating layer may be part of a diffuse layer or it could be a separate structure. The coadsorption of the cations is required to maintain overall charge neutrality. It is in this sense that we refer to the cations as coadsorbed. Phenomena of this type occur frequently in electrochemistry. In a previous paper we very briefly described results for this system in an external applied field corresponding to uncompensated charge on the immersed electrode. In the present calculation the charge on the electrode due to electrostaic images is +|e|. The presence of two adsorbed iodides creates an anisotropic surface electric field and some simulations were run for 3 ns to improve the cation statistics. Even though only small changes in the distribution were observed due to configurations accumulated at later times, we regard the calculated distributions for the cation as being approximate. A prelimary account of the probability distributions of this simulation has been published[39]. This is the first report of the potentials across this cell.

Figure 11 shows the probability density profiles for selected species in solution. There are some similarities in the results for water and the lithium ion for this system and the one discussed in the last section. In particular the water looks quite unstructured compared to hydrated ions, and the Li^+ ion is bimodal. The I^- ion distribution is sharper because the electrode is positively charged.

The initial configuration was a random arrangement of ions and water on a cubic lattice. Both the iodides adsorbed within 50 ps. Note that the iodide distribution is localized at the surface as in the case of one iodide, and the lithium is more diffuse than in the case of a single lithium in the field of its own electrostatic image charge. Except for slightly accentuated broad structures in the range 0.4 to 0.6 nm, the water distribution resembles the distribution already calculated for zero applied field[62]. In particular we note that there are no new peaks near 0.65 nm indicative of localized surface water. The proton H_ST2 and point charge PC_ST2 components have more structure near the metal than in zero field. This is to be expected since they are charged and the field between them and their images is unscreened. The atomic charge density has a deep minimum at ca. 0.7 nm due to iodide and a shoulder at ca. 0.75 nm due to the PC_ST2.

Figure 12 shows the electric potential calculated using the two methods. Starting from the left the monopole potential first rises as it passes through the lithium layer, and then drops rapidly as it approaches the sheet of adsorbed iodide, finally it turns upward because the electrode carries a net positive image charge. Apart from the upward turn near the metal this monopole behaviour is qualitatively similar to that depicted for the model in Figure 1. Our assertion that the traditional models neglect significant contributions from the water can be seen by examination of Figure 12. There is significant structure in the electric potential calculated by either method induced by orientation and packing distribution of the waters at the surface. The monopole term is completely compensated ($-0.65 < z < 0.4$ nm) by the dipole potential from the water molecules as shown by curve m+d until next to the metal surface where water is more strongly oriented and where the water supply drops rapidly to zero. From 0.4 nm to 0.65 nm the atomic potential closely follows that of one iodide (see Figure 6). On the right hand side of Figure 12 we show the potentials atomic (atm), monopole m and m+d+q scaled by a factor 0.1.

Scale up is likely to be an important issue since the size of the system may be too small to allow the diffuse layer lithium ion enough space to distribute without interference from the restraining wall at z=-0.931 nm. However conclusions drawn concerning the behaviour of ions within 1.0 nm of the metal surface will not be very sensitive to the position of the restraining wall. An example of a large system with intact double layer is discussed next.

VIII. 1M NaCl SOLUTION.

In this final example we describe a simulation with approximately 1600 water molecules and ions in a box with edge length L = 3.724 nm. The simulation cell contains 32 Na^+ ions, 28 Cl^- ions, and 1576 water molecules. The NaCl concentration is about 1M. The electrostatic image charge on the electrode surface due to the difference in number of positive over negative ions is -4|e| or 0.046 C m^{-2}. This essentially the same charge density as in all the earlier smaller simulations with non zero electrode charge density. Computer time constraints dictated the use of a simple water model. For this reason we chose the SPCE water model (three charged mass points[66]) over the ST2 water model (two charged mass points, two charged zero mass points, one uncharged mass point). The NaCl parameters[67] used are those appropriate for SPCE water. We also experimented with simulations run at elevated temperatures to increase the diffusion rate of the ions in order to get better statistics. In this calculation the temperature was 30 °C. The simulation was run for 840 ps with the first 100 ps used to equilibrate the system. On a dedicated IBM RS6000 model 550 workstation the calculation takes approximately 10 to 12 weeks.

Figure 13 shows the probability density profiles for the water proton, water mass center, Na^+ ions and Cl^- ions. The anion distribution (broken line) has been smoothed to permit it to be distinguished from the cation. Also shown rising monotonically from the left are the integrals of the ion densities. The near coincidence of the integrals for $z < 0.7$ nm shows that the electrolyte is approximately charge neutral. For $z > 0.7$ nm the integrated densities systematically diverge as expected for a transition from the locally neutral 'bulk' electrolyte into the 'diffuse' part of the electric double layer where screening occurs. At $z = 1.0$ nm the divergence in the integrated densities equals the largest previous difference in the two curves implying that the region $z > 1.0$ nm corresponds to solution shielding the charge on the metal. The Na^+ ion distribution shows well defined structure in the form of a broad peak at ca. 1.1 nm, and a sharp peak at 1.4 nm. The water and proton distributions appear flat for $|z| < 0.8$ nm. On the metal

side the water probability distribution has peaks at 0.9 nm, 1.2 nm, and a strong asymetric peak at 1.6 nm. This latter feature appears to be composite being the superposition of a broad feature at 1.5 nm and a narrow peak at 1.6 nm. The peaks in the proton distribution are at 0.9 nm, 1.2 nm, 1.55 nm, and 1.7 nm. The last peak at ca. 1.7 nm comes from protons in water OH bonds pointing at the metal.

Figure 14 shows the atomic charge density for a bin function with width 0.004655 nm (or L/800). We note that the charge density appears flat for $|z| < 0.8$ nm. The contribution from the ionic charge for $z > 0.8$ nm is not evident because the charge on the waters dominates. The electric field was obtained by integration from $-\infty$ to position z. The field is flat with small variations around zero in the region $|z| < 0.8$ nm. Near the metal the electric field undergoes a series of rapid oscillations as it vears upwards. These oscillations are due to the water structure at the interface. The general rise is due to the excess Na^+ charge in the double layer.

Figure 15 shows the potential calculated using the atom method, and the components of the potential calculated by the molecule method. The contact potential is about -2.0 V, and as in the smaller simulations the potential in the 'bulk-like' zone comes from the water quadrupole. The broken curve labeled m is that from the ionic charge. If the system were truely neutral then curve m would be flat and zero all the way to the beginning of the diffuse layer. Clearly the small charge imbalances seen in Figure 13 do affect shape of the potential curve and may be an exacting criterion with which to judge these larger simulations. The transition to monotonic decrease starting near $z = 0.7$ nm is another indicator of where the diffuse layer begins in this simulation. Note that m+d shows that the dipole potential completely compensates the monopole. Including the quadrupole to give m+d+q shifts the core region downwards by 3 V and brings the molecular calculation of potential into correspondence with the atom method of calculation. The molecular method has larger extrema near the surface compared to the atom method. The reason for this is the very small bin size and the consequential need to include

many high order multipoles in the molecule method. However as required the contact potential is the same in each case. Note also that adding the quadrupole term does not change the contact potential.

In summary this larger simulation has verified that water structure near walls is not an artifact of small size. In 1M NaCl the double layer is about 1 nm thick and encompasses about three layers of water. These water layers can significantly affect the distribution of ions near the metal creating features in the probability distributions that are not describable in the Gouy-Chapman-Stern model.

IX. CONCLUSIONS

In this paper we have shown how the results of molecular dynamics simulations performed at constant N,V,T can be used to calculate the electrostatic field and potential across an electric double layer. Apart from usual molecular dynamics assumptions we used a model for an immersed electrode in which electrode charge was equal to the image charge on the metal. All electrostatics were summed without trunkating the long range coulomb interaction using the fast multipole method. The charge distribution in the system was analysed by two methods. One was based on the charges in atoms in vacuum, the other was based on molecules and required expanding the positions of charge inside a molecule about an origin on each molecule. The later method provided a natural route for decomposing fields into monopole and higher order multipole components. We also showed, by increasing the length scale over which local average is taken, how microscopic structure due to the water probability distribution is systematically washed away leaving only the macroscopic effect of the water dielectric polarization on the electric surface potential. We also showed using the results of a calculation almost an order of magnitude larger in number of water molecules, that the main features evident in smaller calculations of the probability profiles for water near charged metal surfaces are not greatly affected by scale up. This implies that small simulations involving a few hundred water molecules provide a useful starting point for studying double layer properties.

In a series of examples starting with single ions in water, and then to increasingly more complex cases we explored fields close to the surface and across double layers in some electrochemically interesting examples. The case of lithium was chosen to explore some of the consequences of averaging over length scales from smaller to larger than a water molecule. In the final example of 1M NaCl we demonstrated the coexistence of bulk and double layer regions in equilibrium in the same simulation. Since the system contained sixty ions there is a ample correlation between ions and amongst ion and water molecules.

ACKNOWLEDGEMENTS

This research was supported in part by the Office of Naval Research. The contributions of JNG were performed under the auspices of US DOE contract W-7405-Eng-48.

REFERENCES

1 G. Gouy, J. Physique **9**, 457 (1910).

2 D. L. Chapman, Phil. Mag. **25**, 508 (1913).

3 D. L. Chapman, Phil. Mag. **25**, 475 (1913).

4 O. Stern, Z. Elektrochem. **30**, 508 (1924).

5 D. Henderson and M. Plischke, Mol. Phys. **62**, 801 - 804 (1987).

6 L. F. Greengard, *The Rapid Evaluation of Potential Fields in Particle Systems.* (The MIT Press, Cambridge, Massachusetts, 1987).

7 L. Greengard and V. Rokhlin, J. Comp. Phys. **73**, 325-348 (1987).

8 J. Carrier, L. Greengard, and V. Rokhlin, Siam J. Sci. Stat. Comput. **9**, 669-686 (1988).

9 L. Greengard and V. Rokhlin, Chemica Scripta **29A**, 139-144 (1989).

10 J. O. Bockris and A. K. Reddy, *Modern Electrochemistry, Vol.2* (Plenum Press, New York, 1973).

11 J. O. Bockris and A. Gonzalez-Martin, Spectroscopic and Diffraction Techniques in Interfacial Electrochemistry, NATO ASI Series C, Vol. 320 **320**, 1-54 (1990).

12 J. O. Brockris, M. A. Devanathan, and K. Müller, Proc. Roy. Soc.(London) **A274**, 55-79 (1963.).

13 R. W. Hockney and J. W. Eastwood, *Computer Simulation using Particles* (McGraw-Hill, New York, 1981).

14 M. A. Wilson, A. Pohorille, and L. R. Pratt, J. Chem. Phys. **88**, 3281 - 3285 (1988).

15 M. A. Wilson, A. Pohorille, and L. R. Pratt, Chem. Phys. **129**, 209 - 212 (1989).

16 L. D. Landau and E. M. Lifschitz, *Electrodynamics of Continuous Media* (Addison-Welsey, 1960).

17 J. D. Jackson, *Classical Electrodynamics* (Wiley, New York, 1975), pp. 54-62.

18 G. Russakoff, Amer. J. Phys. **38**, 1188-1195 (1970).

19 M. R. Philpott and J. N. Glosli, J. Electrochemical Soc. **142**, L25 - L28 (1995).

20 D. Henderson, *Trends in Interfacial Electrochemistry* (Reidel, Dordrecht, Holland, 1986), p. 183.

21 J. W. Halley, B. Johnson, D. Price, and M. Schwalm, Phys. Rev. B **31 B**, 7695-7709 (1985).

22 J. W. Halley and D. Price, Phys. Rev. B **35 B**, 9095-9102 (1987).

23 D. L. Price and J. W. Halley, Phys. Rev. B **38 B**, 9357-9367 (1988).

24 K. Heinzinger, in *Computer Modeling of Fluids Polymers and Solids,,* edited by C. R. A. Catlow, S. C. Parker, and M. P. Allen (Kluwer, Holland, 1990), Vol. 293, NATO ASI Series C, pp. 357-404.

25 G. Nagy and K. Heinzinger, J. Electroanal. Chem. **296**, (1990).

26 K. Heinzinger, Pure Appl. Chem. **63**, 1733-1742 (1991).

27 J. Seitz-Beywl, M. Poxleitner, and K. Heinzinger, Z. Naturforsch. **46A**, 876 - 886 (1991).

28 G. Nagy and K. Heinzinger, J. Electroanal. Chem. **327**, (1992).

29 J. Seitz-Beywl, M. Poxleitner, M. M. Probst, and K. Heinzinger, Internat. J. Quantum Chem. **42**, 1141 - 1147 (1992).

30 E. Spohr and K. Heinzinger, Ber. Bunsenges. Phys. Chem. **92**, 1358-1363 (1988).

31 E. Spohr and K. Heinzinger, Electrochimica Acta **33**, 1211-1222 (1988).

32 E. Spohr, J. Phys. Chem. **93**, 6171 - 6180 (1989).

33 E. Spohr, Chem. Phys. **141**, 87 - 94 (1990).

34 E. Spohr, Chem. Phys. Let. **207**, 214 - 219 (1993).

35 M. R. Reddy and M. Berkowitz, Chem. Phys. Letters **155**, 173-176 (1989).

36 K. Raghavan, K. Foster, K. Motakabbir, and M. Berkowitz, J. Chem. Phys. **94**, 2110-2117 (1991).

37 L. Perera and M. L. Berkowitz, J. Phys. Chem. **97**, 13803 - 13806 (1993).

38 B. E. Conway, J. O. Bockris, and I. A. Ammar, Trans. Faraday Soc. **47**, 756 - 766 (1951).

39 M. R. Philpott and J. N. Glosli, in *Theoretical and Computational Approaches to Interface Phenomena*, edited by H. Sellers and J. T. Golab (Plenum, New York, 1994), pp. 75 - 100.

40 F. H. Stillinger and A. Rahman, J. Chem. Phys. **60**, 1545-1557 (1974).

41 O. Steinhauser, Mol. Phys. **45**, 335-348 (1982).

42 C. Y. Lee, J. A. McCammon, and P. J. Rossky, J. Chem. Phys. **80**, 4448-4455 (1984).

43 R. A. Friedman and B. Hoenig, Biopolymers **32**, 145-159 (1992).

44 B. E. Hingerty, R. H. Richie, T. L. Ferrel, and J. E. Turner, Biopolymers **24**, 427-439 (1985).

45 P. R. Weiner and P. A. Kollman, J. Comp. Chem. **2**, 287-303 (1981).

46 J. A. McCammon, P. G. Wolynes, and M. Karplus, Biopolymers **18**, 927-942 (1979).

47 B. R. Brooks, R. E. Bruccoleri, B. D. Olafson, D. J. States, S. Swaminathan, and M. Karplus, J. Comp. Chem. **4**, 187-217 (1983).

48 S. J. Weiner, P. A. Kollman, D. A. Case, U. C. Singh, C. Ghio, G. Alagona, S. Profeta Jr, and P. Weiner, J. Amer. Chem. Soc. **106**, 765-784 (1984).

49 G. E. Schacher and F. W. de Wette, Phys. Rev. **136A**, 78-91 (1965).

50 J. A. Barker and R. O. Watts, Mol. Phys. **26**, 789-792 (1973).

51 N. Parsonage and D. Nicholson, J. Chem. Soc. Faraday Trans. 2 **82**, 1521-1535 (1986).

52 N. Parsonage and D. Nicholson, J. Chem. Soc. Faraday Trans. 2 **83**, 663 - 673 (1987).

53 P. P. Ewald, Ann. Physik **54**, 519 (1917).

54 P. P. Ewald, Ann. Physik **54**, 557 (1917).

55 M. Born and K. Huang, *Dynamical Theory of Crystal Lattices* (The Clarendon Press, Oxford, England, 1954).

56 <missing author>, <Missing journal>.

[57] M. A. Wilson, A. Pohorille, and L. R. Pratt, J. Chem. Phys. **90**, 5211 - 5213 (1989).

[58] E. Gileadi, E. Kirowa-Eisner, and J. Penciner, *Interfacial Electrochemistry* (Addison-Wesley, Reading, Massachusetts, 1975).

[59] D. A. Rose and I. Benjamin, J. Chem. Phys. **95**, 6856-6865 (1991).

[60] J. N. Glosli and M. R. Philpott, J. Chem. Phys. **98**, 9995-10008 (1993).

[61] J. N. Glosli and M. R. Philpott, J. Chem. Phys. **96**, 6962-6969 (1992).

[62] J. N. Glosli and M. R. Philpott, in *Microscopic Models of Electrode-Electrolyte Interfaces. Symp. Proc. 93-5*, edited by J. W. Halley and L. Blum (Electrochem. Soc., Pennington, New Jersey, 1993), pp. 90-103.

[63] S. D. Argade and E. Gileadi, in *Electroadsorption*, edited by E. Gileadi (Plenum, New York, 1967), pp. 87-115.

[64] M. R. Philpott, J. N. Glosli, and S. Zhu, Surface Sci. **335**, 422 - 431 (1995).

[65] L. D. Landau and E. M. Lifschitz, *Electrodynamics of Continuous Media* (Addison-Welsey, 1960), pp. 99 - 101.

[66] H. J. Berendsen, J. R. Grigera, and T. P. Straatsma, J. Phys. Chem. **91**, 6269 - 6271. (1987).

[67] R. W. Impey, P. A. Madden, and I. R. McDonald, J. Phys. Chem. **87**, 5071 - 5083 (1983).

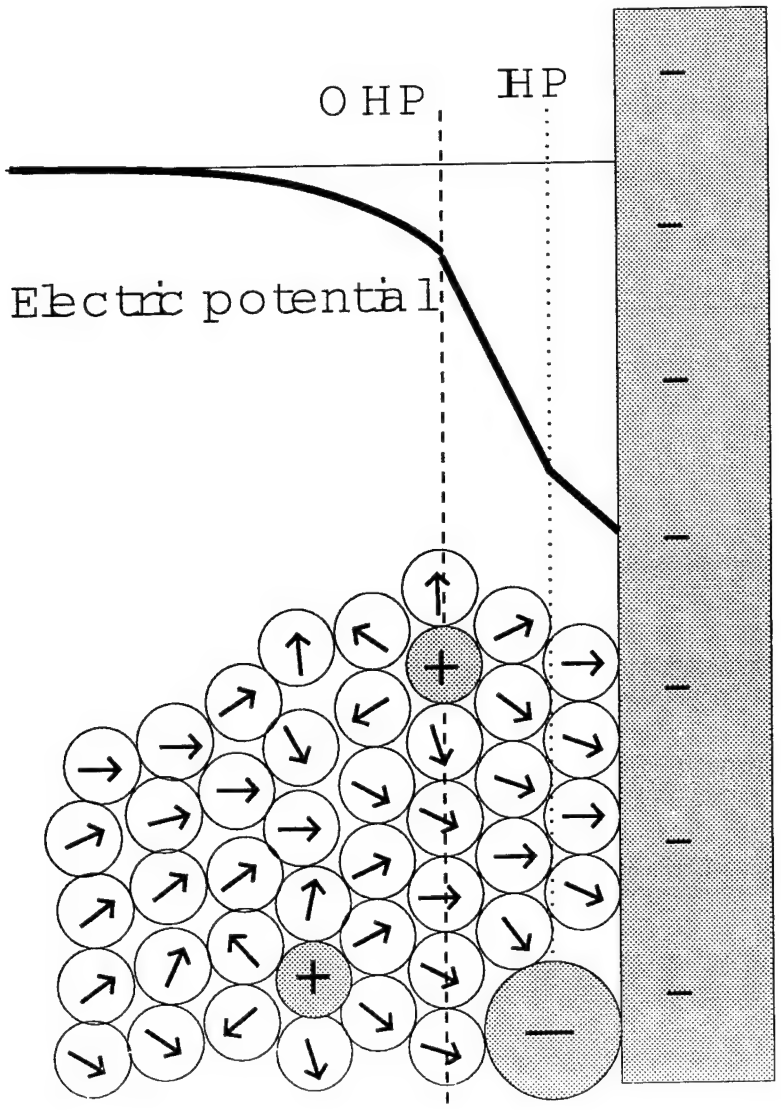

Figure 1. Schematic diagram of the traditional view of the electric double layer showing a flat negatively charged electrode with contact adsorbed anion and fully hydrated cations at the outer Helmholtz plane (OHP). Electric potential shown schematically at the top.

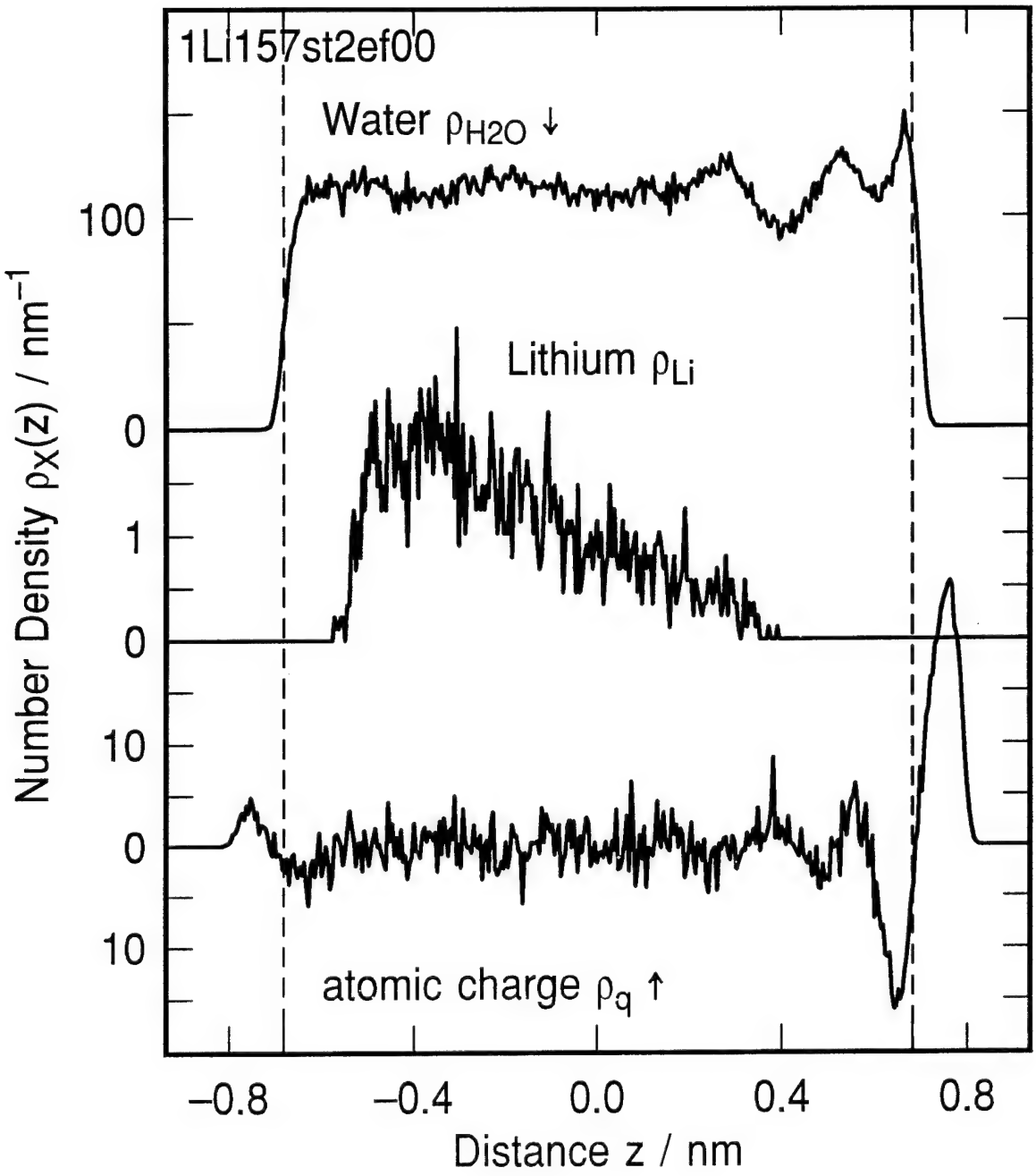

Figure 2. Density profiles for lithium cation Li^+ ion, 157 ST2 waters and the total atomic charge density ρ near an immersed electrode. Image charge on metal -1 is screened by the Li^+ ion. Metal electrode on right hand side, restraining wall on the left. Image plane at z = 0.931 nm. Wall potentials go through zero at |z|=0.682 nm. Simulation from 100 ps to 2500 ps.

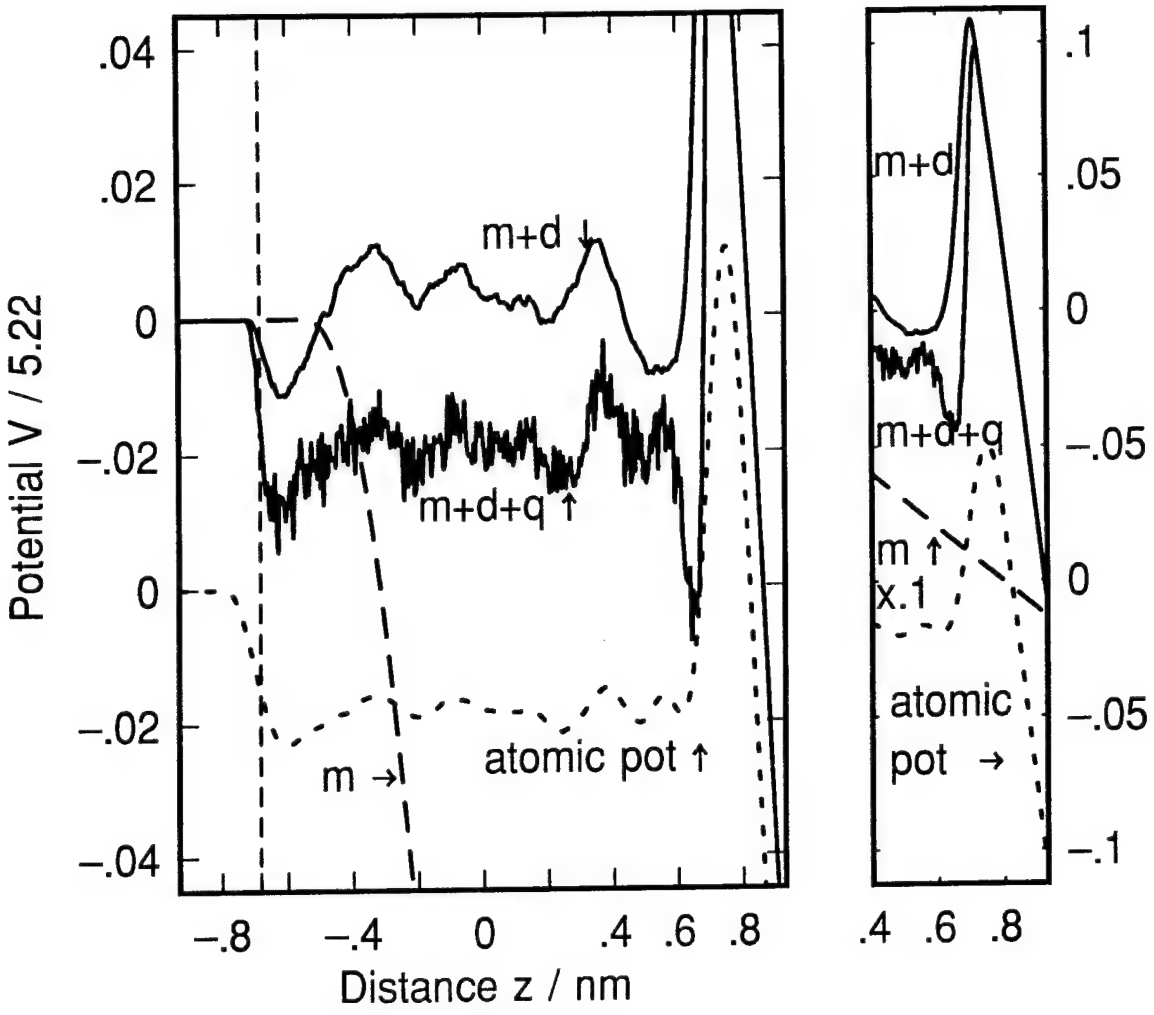

Figure 3. Potential drop across the system Li^+ ion and 157 ST2 waters in the immersed electrode model. Calculations using atom and molecule methods. Bin size 0.004655 nm. Molecule method: m monopole only, m+d monopole and dipole, m+d+q monopole dipole and quadrupole. The right side panel shows the potentials on larger scale for z > 0.4 nm, with the monopole scaled by 0.1. Image charge on metal -1 is screened by the Li^+ ion. Metal electrode on right hand side, non metallic restraining wall on the left. Image plane at z = 0.931 nm. Wall potentials go through zero at |z|=0.682 nm.

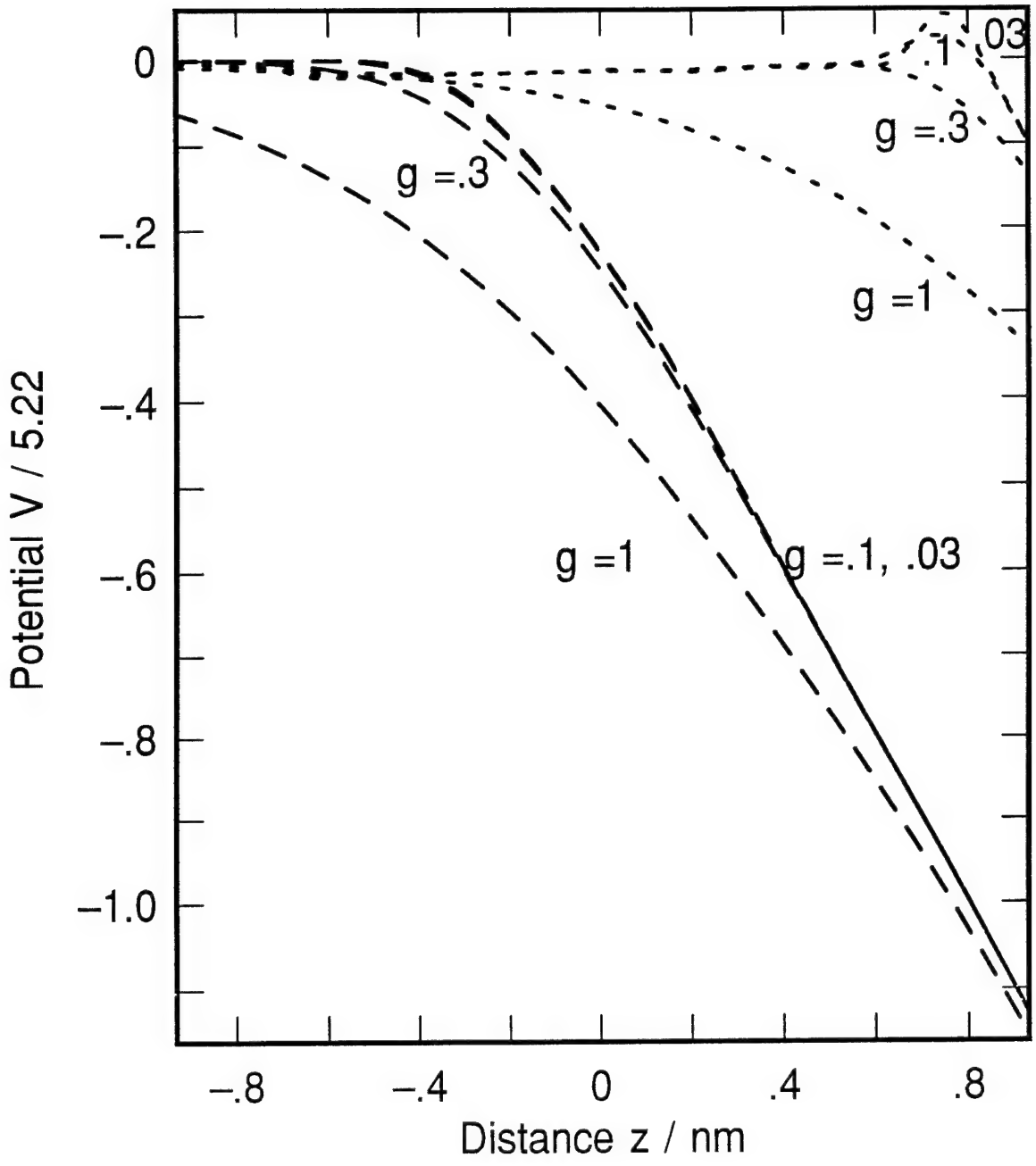

Figure 4. Potential drop across the system Li^+ ion and 157 ST2 waters in the immersed electrode model. Calculations using atom and molecule methods with gaussian widths g = .03, .1, .3, 1.0 nm. Curves for monopole potentials (broken lines) and the total potential by the atom (dotted lines) method. Oscillations in the atomic potential clearly visible in Figure 3 for z > 0.2 nm are washed out on the scale of a water molecule g = .3.

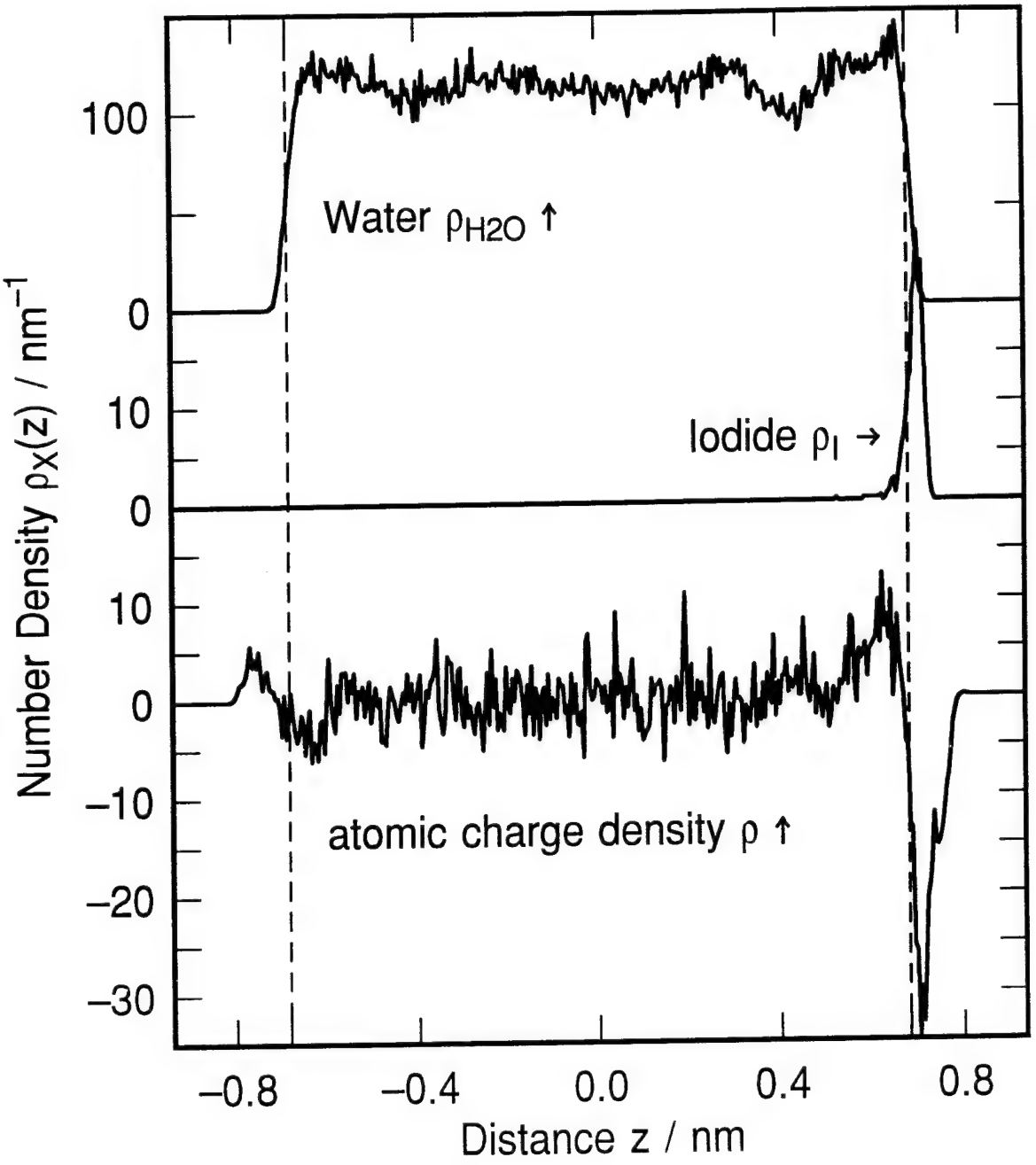

Figure 5. Density profiles for iodide anion I^- ion, 157 ST2 waters and the total atomic charge density ρ near an immersed electrode. Image charge on metal +1 is screened by the I^- ion. Metal electrode on right hand side, restraining wall on the left. Image plane at z = 0.931 nm. Wall potentials go through zero at |z|=0.682 nm.

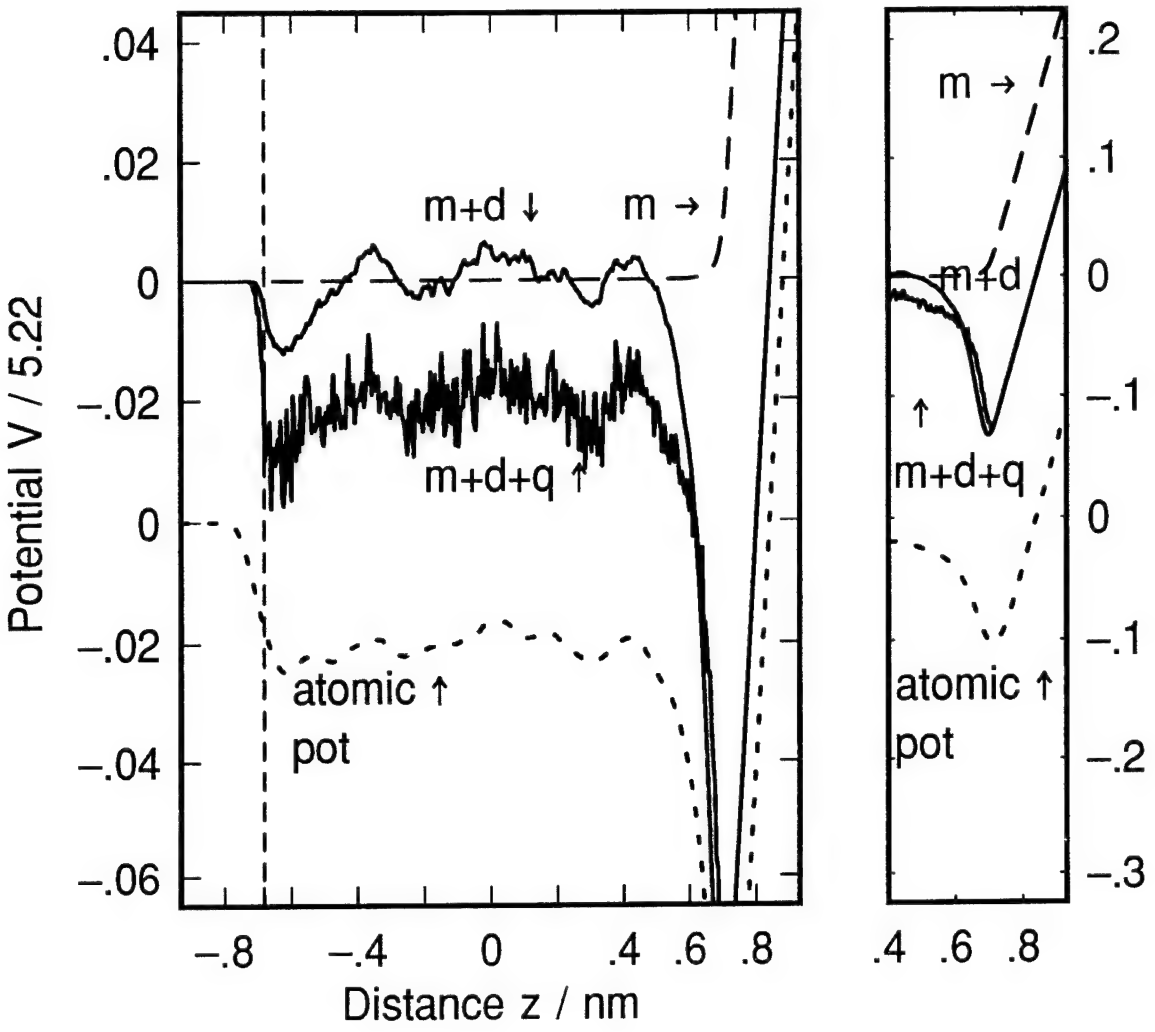

Figure 6. Potential drop across the system I^- ion and 157 ST2 waters in the immersed electrode model. Calculations using atom and molecule methods. Bin size 0.004655 nm. Molecule method: m monopole only, m+d monopole and dipole, m+d+q monopole, dipole and quadrupole. Panel on the right hand side shows the curve for z > 0.4 nm on a reduced scale. Image charge on metal +1 is screened by the I^- ion. Metal electrode on right hand side, restraining wall on the left. Image plane at z = 0.931 nm. Wall potentials go through zero at |z|=0.682 nm.

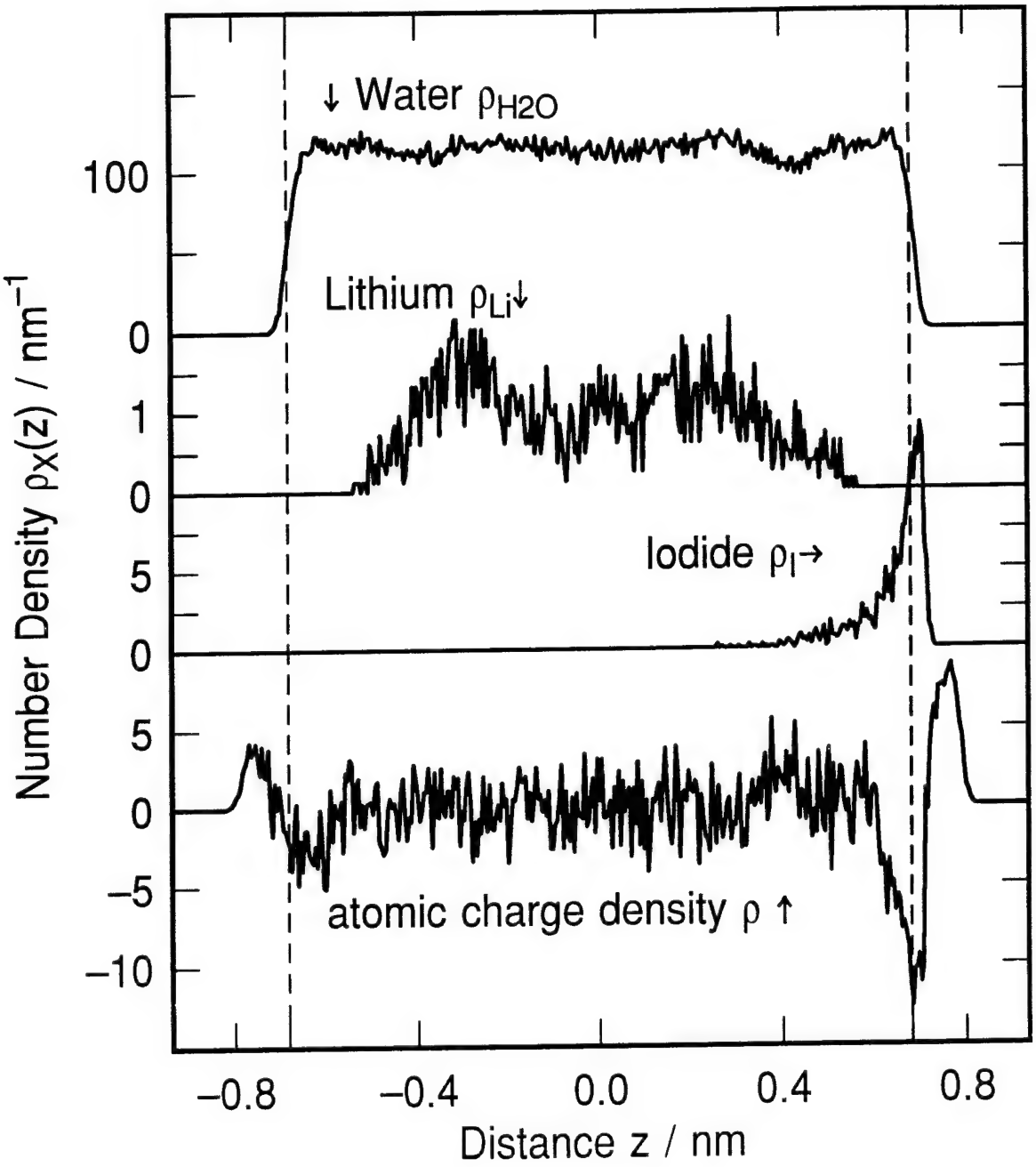

Figure 7. Density profiles a neutral solution consisting of one lithium cation Li^+, iodide anion I^-, and 157 ST2 waters and the total atomic charge density near an immersed electrode. Metal electrode on right hand side, restraining wall on the left. Image plane at z = 0.931 nm. Wall potentials go through zero at |z|=0.682 nm.

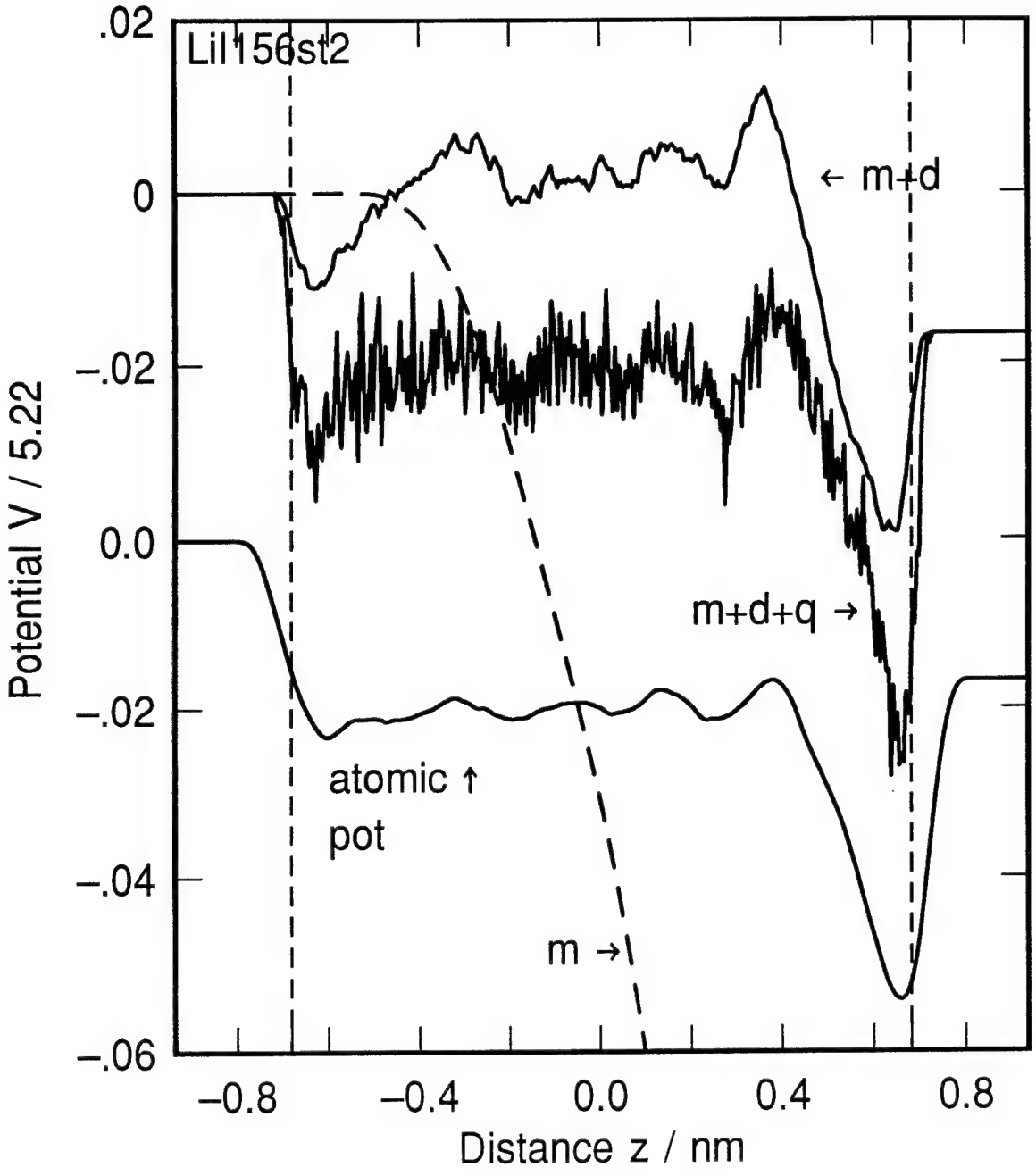

Figure 8. Electric potential drop across a the neutral solution consisting of one lithium ion Li^+, one iodide ion I^-, and 156 ST2 waters next to an immersed electrode. Potential due to atom method shifted by -0.04. Potential from: ions only m, ions and water dipoles m+d, ions and water dipole and quadrupole m+d+q. Note that the potential m+d+q is almost the same as calculated from atomic charges. There is no net image charge on the metal. Metal electrode on right hand side, restraining wall on the left. Image plane at z = 0.931 nm. Wall potentials go through zero at |z|=0.682 nm.

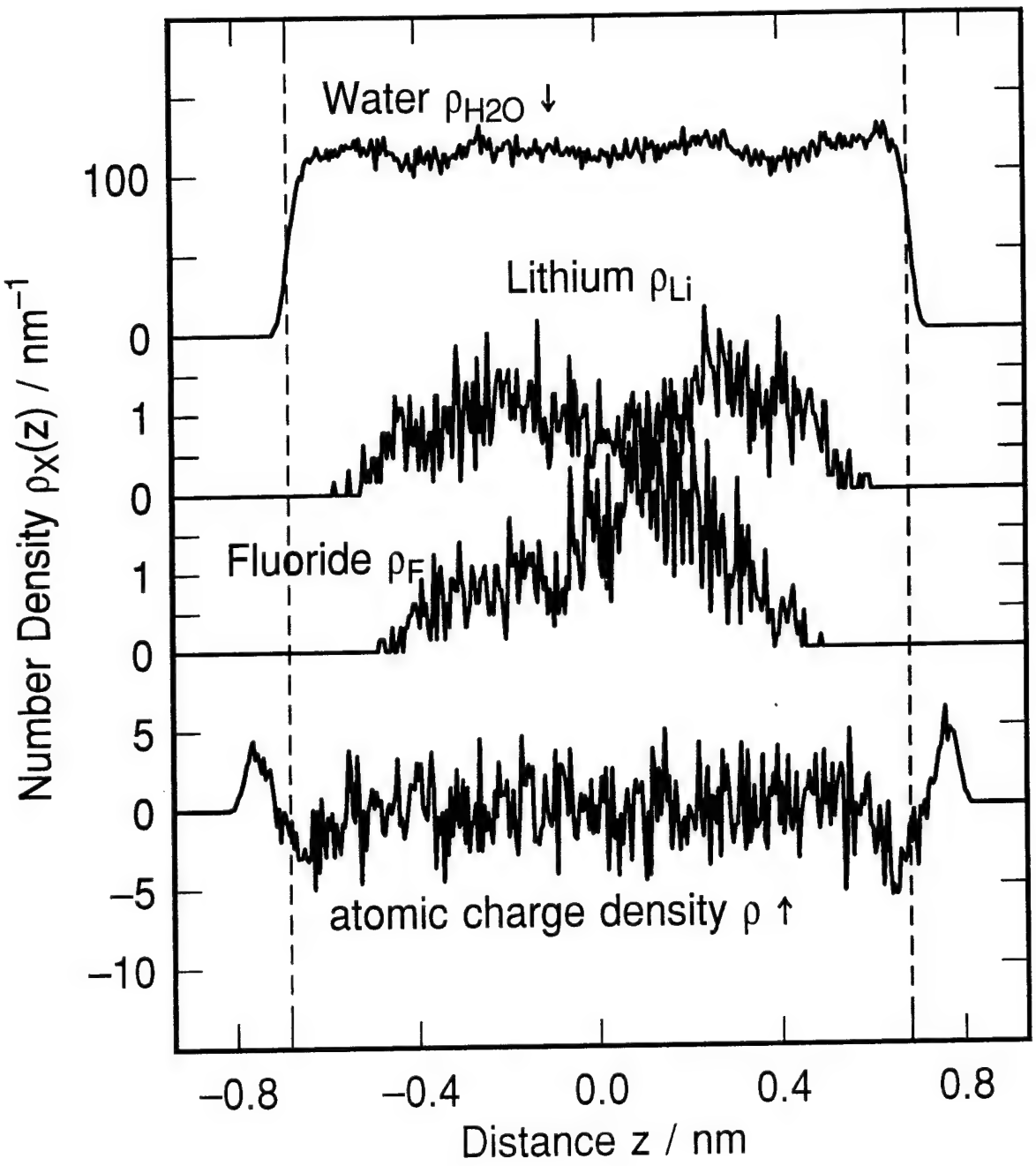

Figure 9. Density profiles for a neutral solution consisting of one lithium ion Li^+, one fluoride ion F^-, and 156 ST2 waters and the total atomic charge density ρ near an immersed electrode. Image charge on metal is zero. Metal electrode on right hand side, restraining wall on the left. Image plane at z = 0.931 nm. Wall potentials go through zero at |z|=0.682 nm.

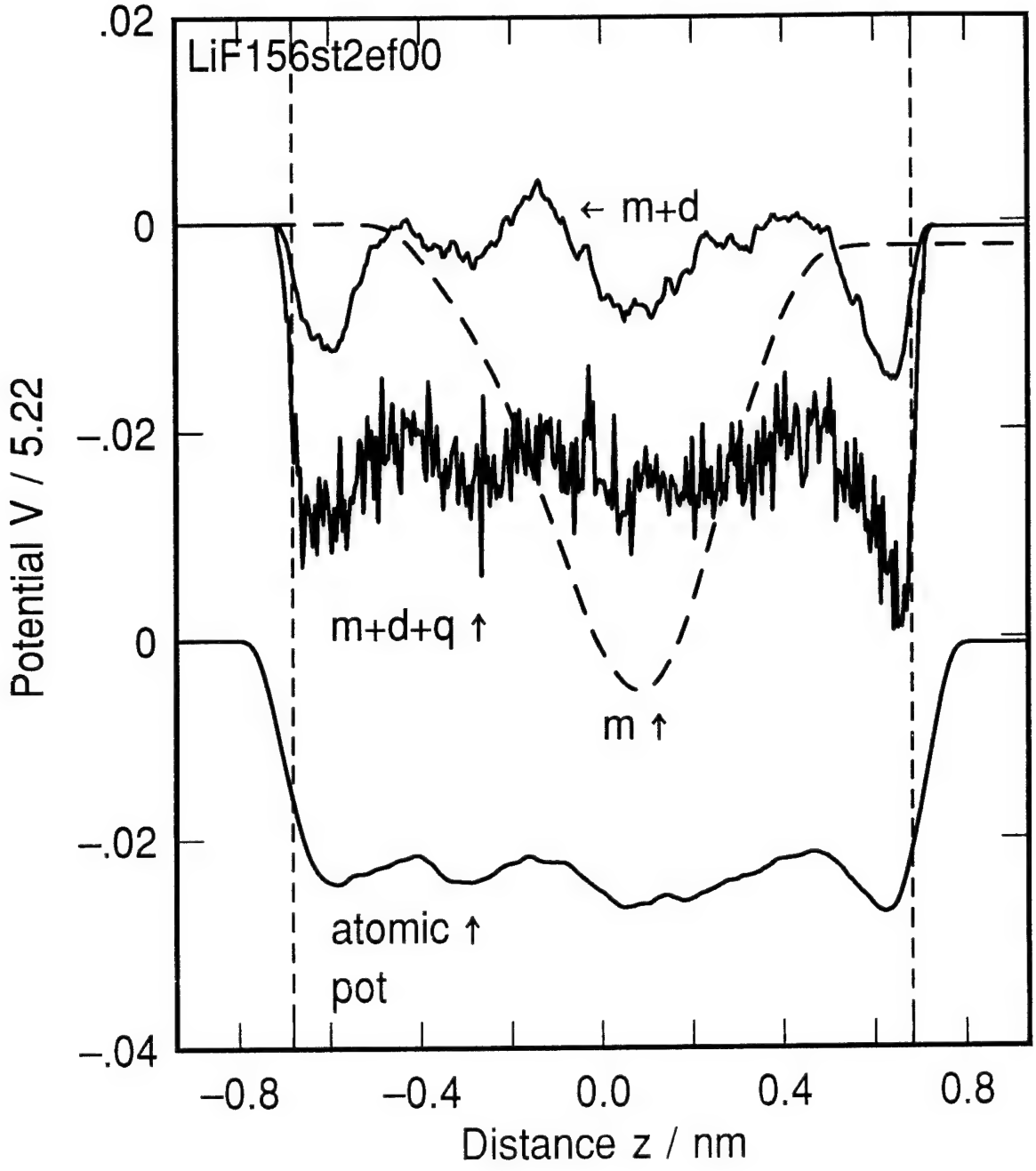

Figure 10. Electric potential drop across a neutral solution consisting of one lithium ion Li^+, one fluoride ion F^-, and 156 ST2 waters next to an immersed electrode. Potential due to atom method is shifted by -0.04. Potential from: ions only m, ions and water dipoles m+d, ions and water dipole and quadrupole m+d+q. Note that the potential m+d+q is almost the same as calculated from atomic charges. Metal electrode on right hand side, restraining wall on the left. Image plane at z = 0.931 nm. Wall potential goes through zero at |z|=0.682 nm.

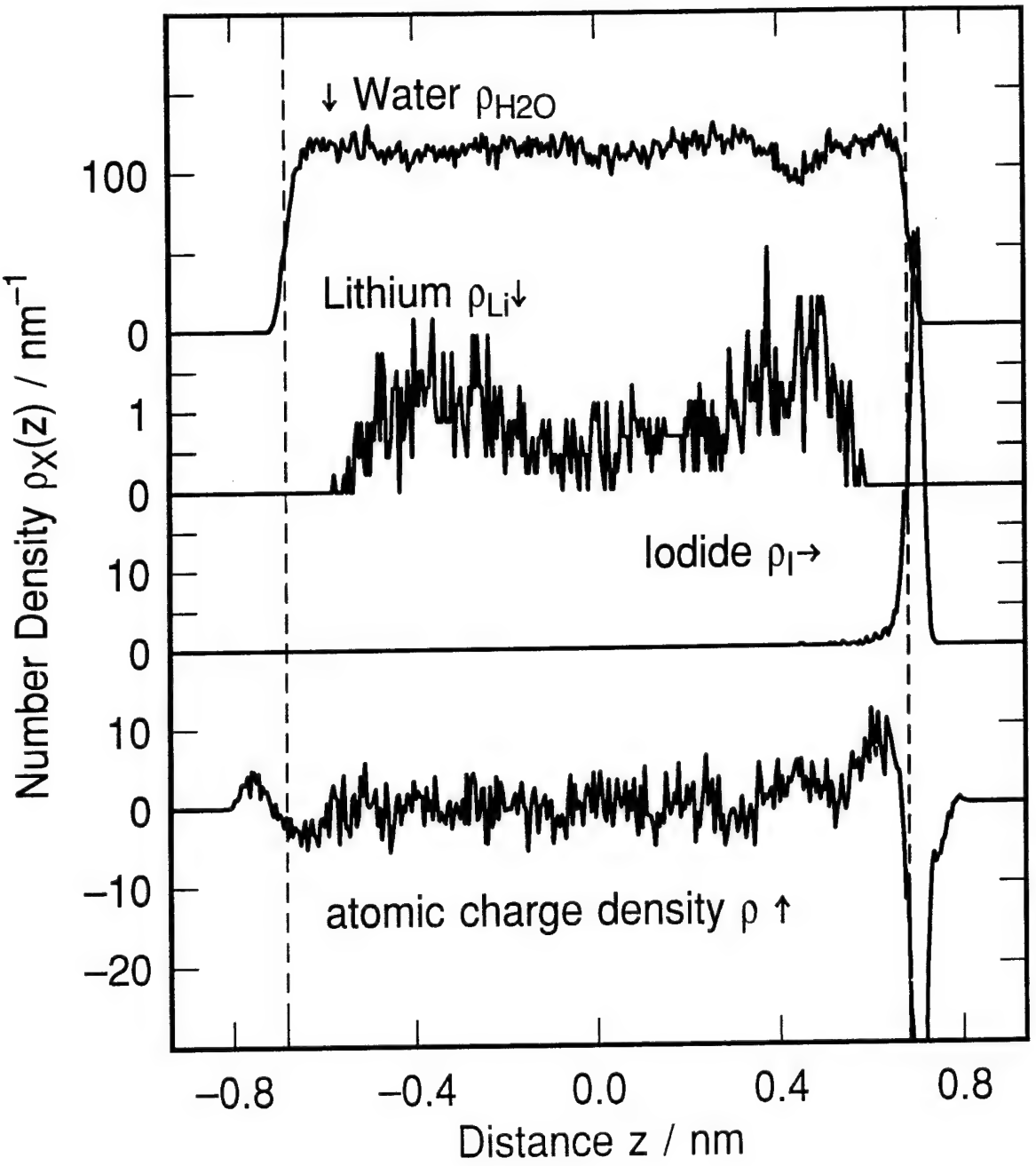

Figure 11. Density profiles for two I^-, one lithium cation Li^+, 155 ST2 water molecules and total atomic charge density next to an immersed electrode. The net image charge on the metal +1 is screen by three ions in solution.

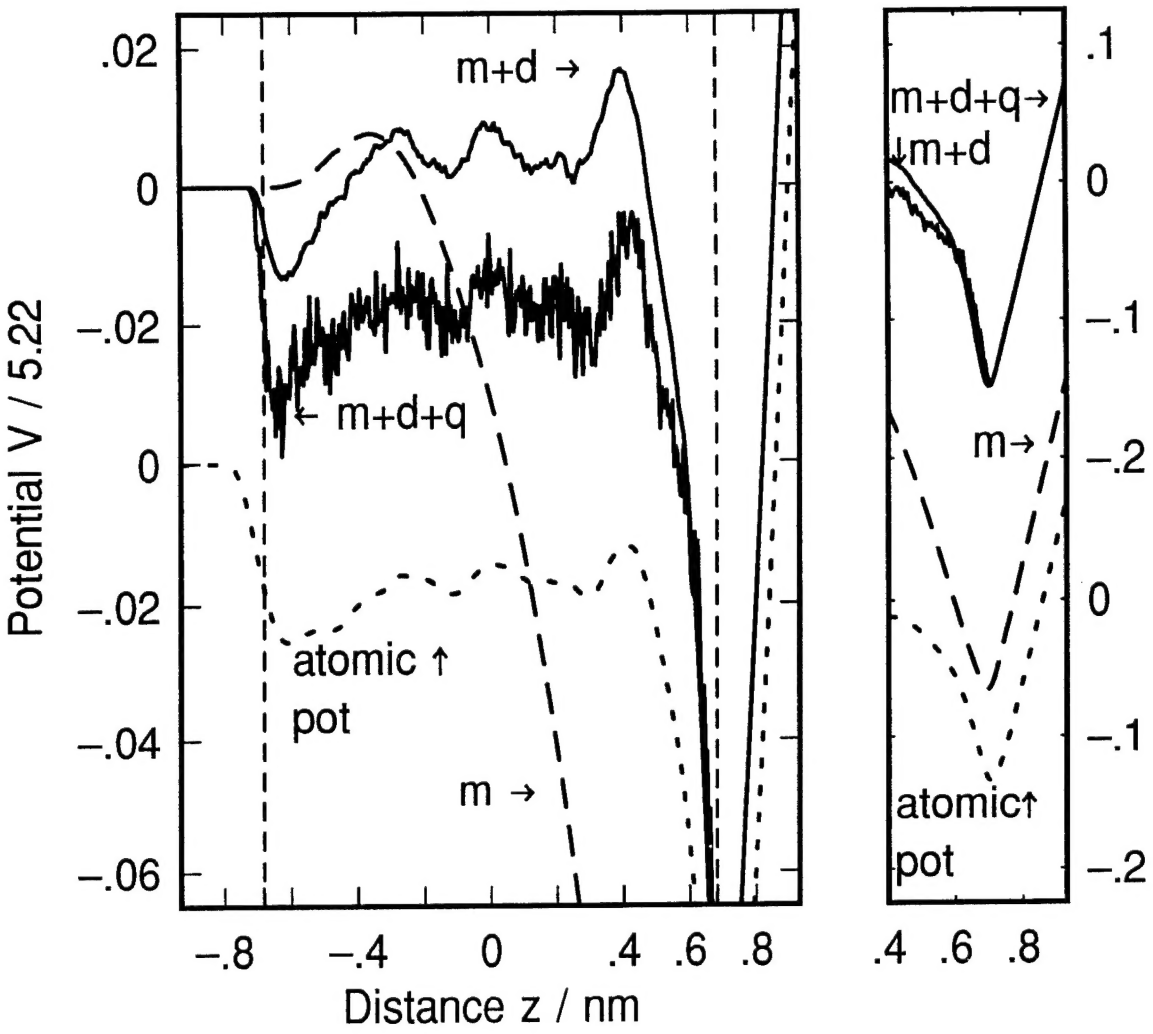

Figure 12. Electric potential drop across a charged solution consisting of one lithium ion Li^+, two iodide ions I^-, and 155 ST2 waters next to an immersed electrode. Potential due to atom method is shifted by -0.04. Potential from: ions only m, ions and water dipoles m+d, ions and water dipole and quadrupole m+d+q. Note that the potential m+d+q is almost the same as calculated from atomic charges. Metal electrode on right hand side, restraining wall on the left. Image plane at z = 0.931 nm. Wall potential goes through zero at |z|=0.682 nm. Panel on right shows potentials for z > 0.4 nm on a scale x5 larger than the left side.

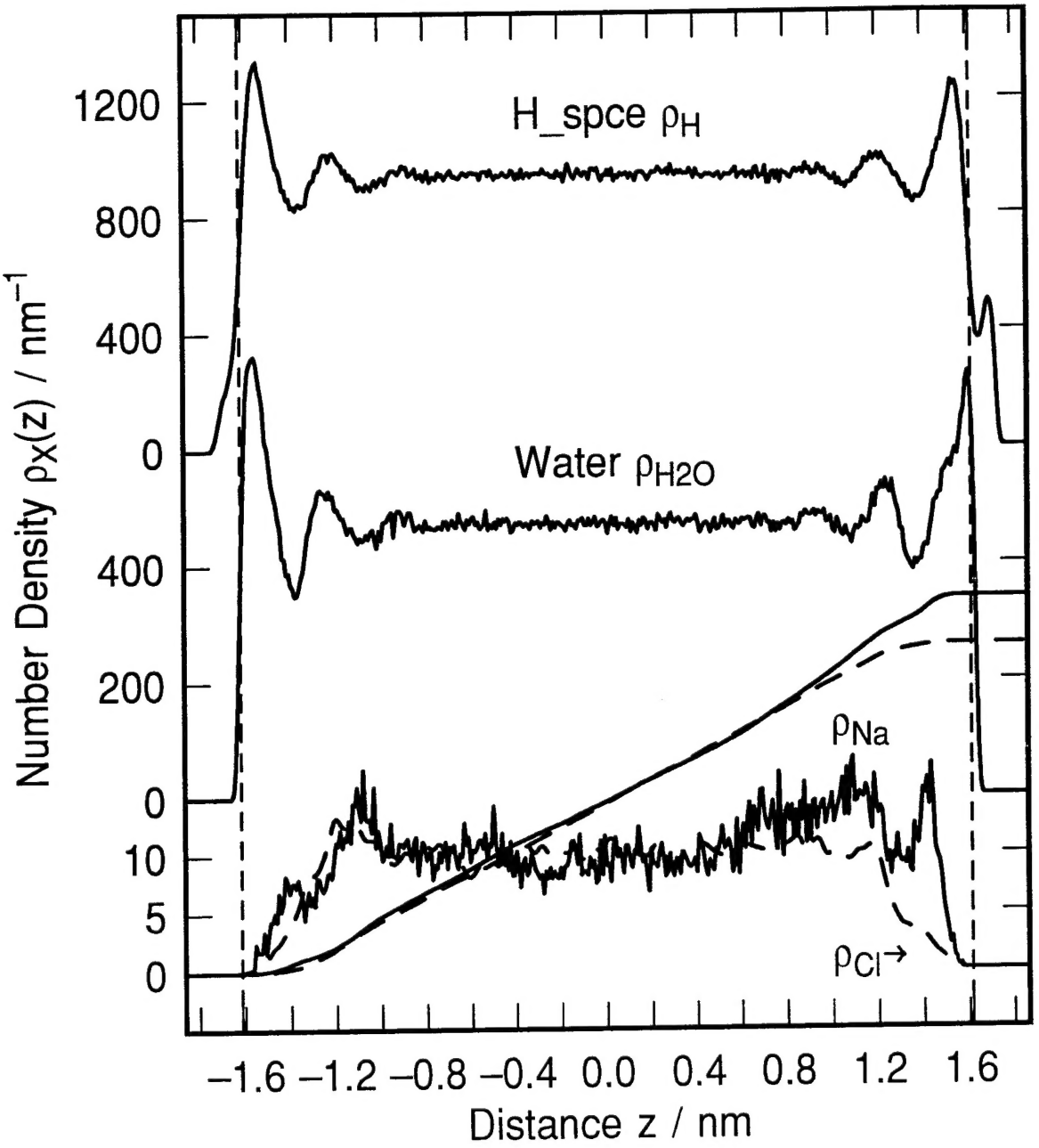

Figure 13. Screening for 1M NaClaq at 30 °C. Electrolyte composition: 32 Na^+ ions, 28 Cl^- ions, and 1576 SPCE water molecules near an immersed electrode. Image charge on the metal -4|e|. Metal electrode on right hand side at z = 1.862nm (position of image plane), restraining wall origin on the left at z = -1.862 nm, wall potentials on both sides of the simulation cell go through zero at |z|= 1.615 nm. Simulation duration 100 ps to 840 ps.

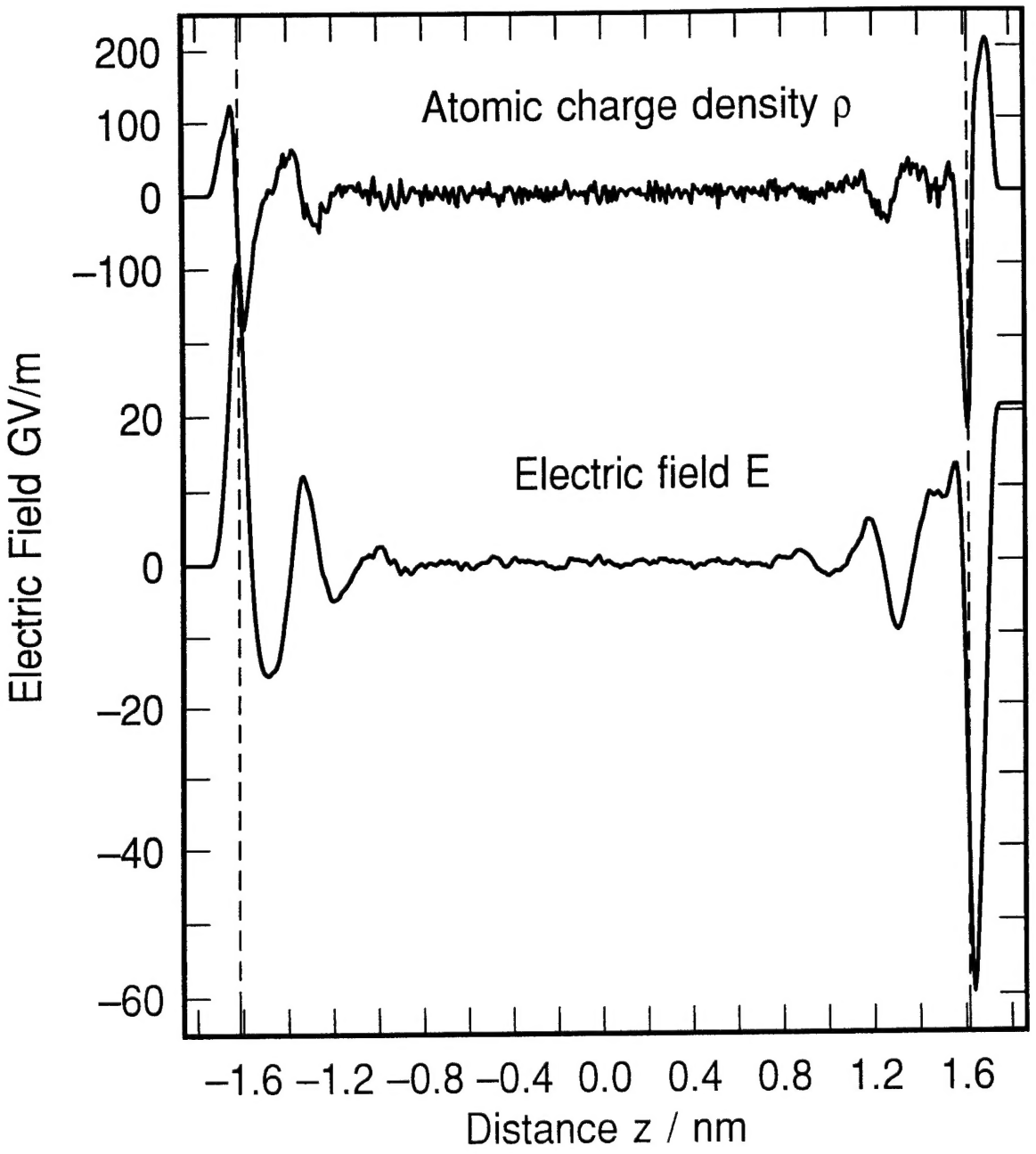

Figure 14. Vacuum charge density, electric field and potential for 1M NaClaq at 30 °C and -4e image charges. Electrolyte composition: 32 Na^+ ions, 28 Cl^- ions, and 1576 SPCE water molecules near an immersed electrode. Metal electrode on right hand side at z = 1.862nm (position of image plane), restraining wall origin on the left at z = -1.862 nm, wall potentials on both sides of the simulation cell go through zero at |z|= 1.615 nm. Simulation duration 100 ps to 840 ps.

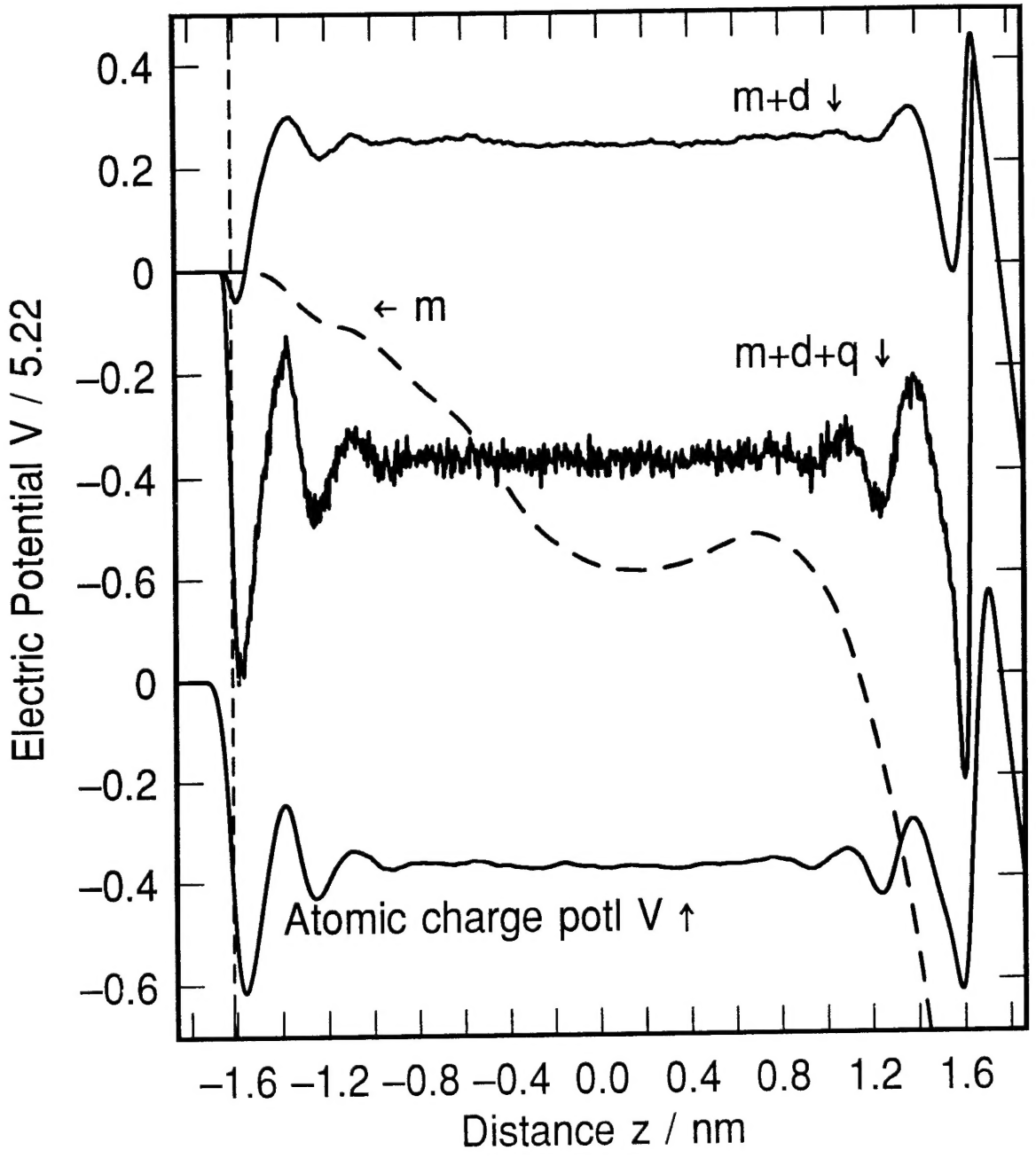

Figure 15. Electric potential drop across a charged solution consisting of for 1M NaCl solution at 30 °C and -4|e| image charge on the metal. Potential calculated by the atom method is shifted by -0.8. Molecule method potentials from: ions only m, ions and water dipoles m+d, ions and water dipole and quadrupole m+d+q. Note that the potential m+d+q is almost the same as calculated by the atom method. The net image charge on the metal -4|e| is screened by a total of sixty ions. Electrolyte composition: 32 Na^+ ions, 28 Cl^- ions, and 1576 SPCE water molecules near an immersed electrode. Metal electrode on right hand side at z = 1.862nm (position of image plane), restraining wall origin on the left at z = -1.862 nm, wall potentials on both sides of the simulation cell go through zero at |z|= 1.615 nm. Simulation duration 100 ps to 840 ps.